Marine and Petroleum Geology 148 (2023) 106020

Contents lists available at ScienceDirect

Marine and Petroleum Geology

journal homepage: www.elsevier.com/locate/marpetgeo

Diagenesis- and thermal maturity-evolution of the Silurian unconventional hydrocarbon deposits (Tassili n'Ajjer plateau, Algeria): Clay mineralogy, graptolite reflectance, and K–Ar dating

Hocine Djouder [a,b,c,*], I. Tonguç Uysal [d,e], Anne-Christine Da Silva [a], Julien Bourdet [c], Andrew Todd [c], Erick Ramanaïdou [c], Bachir Lamouri [f], Peter Crosdale [g], Frédéric Boulvain [a]

[a] Sedimentary Petrology, University of Liège, B20, Quartier Agora, Allée du Six Août, 12, 4000 Liège, Belgium
[b] Institute of Geological Sciences, Polish Academy of Sciences, Research Centre in Kraków, Senacka 1, 31-002 Kraków, Poland
[c] CSIRO, Australian Resources Research Centre, P.O. Box 1130, Kensington, 6151 Perth, Australia
[d] Department of Geological Engineering, Istanbul University-Cerrahpaşa, 34098 Istanbul, Turkey
[e] School of Earth and Environmental Sciences, The University of Queensland, Brisbane, 4072 Queensland, Australia
[f] Laboratory of Geodynamics and Natural Resources, University of Badji Mokhtar Annaba, BP 12, Sidi Ammar, 23000, Annaba, Algeria
[g] Energy Resources Consulting Pty Ltd, ERC Technologies Pty Ltd, 4/55 Clarence St, Coorparoo, 4151 Queensland, Australia

ARTICLE INFO

Keywords:
Algeria
Silurian
Shale gas and oil
Petroleum source rocks
Diagenesis
Illite
Thermal maturity
Graptolite reflectance

ABSTRACT

The need for determining the thermal maturity of Lower Paleozoic rocks has increased with the intensified unconventional shale oil/gas resources exploration within North Africa, Arabian Peninsula, and the adjoining regions. Indeed, Lower Paleozoic strata represent an increasingly important resource that is related to the globally widespread occurrence of graptolite-bearing marine sediments in an expansive shelf area of the Gondwana. However, some crucial information for basin analysis remains poorly understood even across the largest hydrocarbon-producing province in Algeria.

The present study provides a solid understanding of the diagenesis- and thermal maturity-evolution from the Tassili n'Ajjer plateau while involving multiple and independent approaches, such as clay mineralogy, petrography, graptolite reflectance, source rock maturity, as well as illite K−Ar geochronology. The combined use of X-ray analysis and field emission scanning electron microscope evidenced kaolinite, illite, and iron-rich chlorite as the main authigenic mineral phases. K−Ar data indicate that episodic *in situ* illite crystallization occurred at different times, the oldest illite at about 335 Ma and the youngest illite between 238 and 179 Ma, under diagenetic-to-hydrothermal conditions. Paleotemperature estimates (~165–232 °C) derived from illite crystallinity (0.37–1.58 $\Delta^{\circ}2\theta$), and graptolite reflectance (VR_{eqv}, 1.09–1.84%) values indicate deep diagenetic-low anchizone boundary conditions. This is broadly suggestive of late oil-to-dry gas zones of hydrocarbon generation and destruction, notably in the western sector of the study area.

At least two heating events and diagenetic fluid flow processes are identified mainly in response to various tectonic events. They are largely due to fault reactivations, and migration of hot, potassium-rich, fluids throughout the Phanerozoic. Additionally, these events and processes had a later influence on the hydrocarbon maturation, migration, and/or entrapment, especially along the inherited N–S lineaments and Hoggar Massif mega-shear zones in the westernmost part of the Tassili n'Ajjer plateau.

Lastly, it is important to highlight that the promising areas offering the highest potential for future unconventional hydrocarbon resource exploration could be most likely those bordering major lineaments, coupled with subsequent igneous activity, where unrestricted hydrothermal fluids are frequently reported, as well as the maturation, being much more advanced.

* Corresponding author: Institute of Geological Sciences, Polish Academy of Sciences, Research Centre in Kraków, Senacka 1, 31-002 Kraków, Poland. H.Djouder@ingpan.krakow.pl ; Hocine.Djouder@uliege.be.
E-mail address: Hocine.Djouder@uliege.be (H. Djouder).

https://doi.org/10.1016/j.marpetgeo.2022.106020
Received 8 April 2022; Received in revised form 7 November 2022; Accepted 9 November 2022
Available online 23 November 2022

1. Introduction

The Lower Paleozoic graptolite-bearing marine strata, e.g., the Early Silurian Oued Imihrou black 'hot' shales, are one of the principal hydrocarbon sources that formed oil and gas fields in Paleozoic deposits in many North African intracratonic basins and around the world (MacGregor, 1998; Lüning et al., 2000; Luo et al., 2020). Globally, oil-and-gas source rocks of the Ordovician and Silurian ages, which are mostly graptolite shales, produced up to 9% of all the world's known hydrocarbon reserves discovered by the late 20th century (Klemme and Ulmishek, 1991). It is believed that Silurian graptolite shales produced 80–90% of the Paleozoic-sourced hydrocarbon accumulations stored in the giant oil fields of North Africa and the Arabian Peninsula (Klemme and Ulmishek, 1991; Craig et al., 2008).

Recently since the increasing interest in unconventional shale oil/gas resources, a greater focus and priority is given to better understanding and exploiting the Silurian source rock potential, principally from the largest hydrocarbon-producing province in Algeria (Kuuskraa et al., 2011). Although previous studies have shed light on trace fossil analysis, as well as the sedimentological and sequential framework of the Silurian succession (e.g. Beuf et al., 1971; Bekkouche, 1992; Fekirine and Abdallah, 1998; Lüning et al., 2000; Eschard et al., 2005; Galeazzi et al., 2010; Djouder et al., 2018; Djouder, 2019), some important information on the thermal history in numerous Saharan basins remains poorly understood and still not yet available for natural resources exploration. History of large-scale tectonic and thermal events within the Berkine – Ghadames and Illizi "BGI" basins not only controls directly the distribution of maturation of source rocks but also hydrocarbon generation in time-space, therefore, helping better determination of potential locations for drilling hydrocarbon wells, thus rising confidence in efficient petroleum exploration and development programs.

The primary objective of this study, across the Tassili n'Ajjer plateau, is to fill a significant gap in the research on diagenesis- and thermal-history, which appear to be strongly influenced by major inherited N–S lineaments and the Hoggar Massif mega-shear zones. Also, the present study aims to systematically investigate the Early Silurian Oued Imihrou black 'hot' shales and the overlying Mid−Silurian sandstone levels of the Atafaïtafa Formation, across three separate outcrop analogs while involving multiple techniques and independent approaches, such as clay mineralogy, SEM petrography, organic matter content via petrography and programmed pyrolysis, as well as K−Ar age dating of clay content. The combination of different techniques is essential in providing constraint of a basin's thermal history, since the reliability and consistency of each indicator, i.e., the so-called geo-thermometers, can be limited by many factors during burial diagenesis (Hoffman and Hower, 1979; Espitalié et al., 1985; Eslinger and Pevear, 1988; Kübler and Jaboyedoff, 2000; Meunier, 2005; Ferreiro Mählmann et al., 2012). Indeed, in this study, the combined use of inorganic clay minerals, illite geochronology, and graptolite organic matter is demonstrated successfully, which is crucial, especially in deciphering the thermal evolution of any sedimentary basins hosting significant hydrocarbon potential.

Regarding the structural evolution, results of the present study provide clear evidence of the relationship between authigenic clay minerals precipitation, and the geologically meaningful events in south-eastern Algeria. Specifically, this study presents the first documentation of the reactivation of the Pan-African N–S fault zones in association with large-scale hydrothermal activities that affected the westernmost part of the Tassili n'Ajjer plateau. Illite K−Ar ages are used to evaluate the hydrocarbon generation and emplacement history, especially along the inherited but repeatedly reactivated Hoggar Massif mega-shear zones during the Phanerozoic orogeneses and rifting phases.

2. Geological background

2.1. Regional geology and geological events

Several intracratonic sag basins described at the Algerian Saharan platform contain very thick sedimentary succession. They recorded nearly the entire Phanerozoic history, spanning from the Pan-African orogeny until the recent Alpine orogeny. From west to east, the following basins or sub-basins of different wavelengths from 75 to 620 km may be recognized (Fig. 1A): the Tindouf, Bechar, Reggane, Sbaa, Timimoun, Ahnet, Mouydir, Oued Mya, Berkine – Ghadames and Illizi petroliferous basins (Beuf et al., 1971; Boote et al., 1998). Exceptionally, Paleozoic sediments of the latter basins outcrop in south-eastern Algeria within the Tassili n'Ajjer plateau and are laterally traceable over kilometers (Fekirine and Abdallah, 1998; Djouder et al., 2018).

According to Galushkin and Makhous (2006), the thermal and tectonic evolution of the south-eastern part of the Algerian Saharan platform is closely related to the geologic history of the Hoggar Massif (Touareg Shield). This shield was assembled during the end of the Neoproterozoic (600 Ma), following collisional tectonics during the Pan-African orogeny, between two major Archean-Paleoproterozoic cratons; the Saharan Metacraton and the West African Craton to the east and west, respectively (Abdelsalam et al., 2002; Liégeois et al., 2005, 2013). This collision also produced a large north-south intraplate deformational belt of lithospheric scale, the intrusion of granites, wide folds, faults, and lateral displacement along the inherited Pan-African N–S lineaments (Boudjema, 1987; Guiraud et al., 2000, 2005; Haddoum et al., 2001; Liégeois et al., 2013). It is also important to mention that these preexisting regional-scale extensional mega-shear zones, which seem to be of crustal scale, were repeatedly reactivated during the Phanerozoic orogeneses and riftings (Liégeois et al., 2005; Derder et al., 2016). Therefore, these reactivations led to differentiated subsidence within the surrounding basins, e.g., Berkine – Ghadames and Illizi "BGI" basins, as well as the emersion of some geological structures, e.g., Amguid-El Biod-Messaoud axis, Tihemboka and Ahara Arch (Takherist, 1990; Eschard et al., 2010; Djouder et al., 2015). Following the Paleozoic-Mesozoic, Tertiary tectonic evolution was marked by the sudden slowdown of the African plate throughout the Eocene, hence, inducing large-scale intraplate uplift and exhumation of the whole Touareg Shield (Liégeois et al., 2005, 2013; Rougier et al., 2013). This strong relief evolution of the uplifted dome has removed between 2 and 5 km of overburden strata from the region along the northern margin of the Hoggar, i.e., Tassili n'Ajjer plateau (Craig et al., 2008; Rougier et al., 2013; English et al., 2016).

A more detailed presentation of the geologic setting, tectonic evolution, deposition environment, and deposition model of the southern Algerian Saharan platform can be found in Fekirine and Abdallah (1998); Lüning et al. (2000); Carr (2002); Fabre (2005); Craig et al. (2008); Djouder et al. (2018); Djouder (2019); Perron (2019).

2.2. Study area and samples

The study area is located in the Tassili n'Ajjer plateau of Algeria in the south-eastern part of the Algerian Saharan platform near the Hoggar Massif (Fig. 1B). Outcrops along the Tassili n'Ajjer area offer exceptional exposure to Silurian sections and, more specifically, the organic-rich shales of the Oued Imihrou Formation (see Djouder et al., 2018). Furthermore, the Tassili n'Ajjer plateau is the southern margin of the largest petroliferous BGI basins that provide critical insight in understanding the diagenesis- and thermal maturity-evolution, during the burial history, mainly of the graptolitic Early Silurian, which are the world-class source rock of Paleozoic sourced hydrocarbons, e.g., in North Africa, Middle East and East Asia (e.g. MacGregor, 1998; Lüning et al., 2000; Kuuskraa et al., 2011; Luo et al., 2016, 2020).

The 410 m-thick Silurian strata in the Tassili n'Ajjer plateau are subdivided into the Oued Imihrou Formation, overlaid by the Atafaïtafa

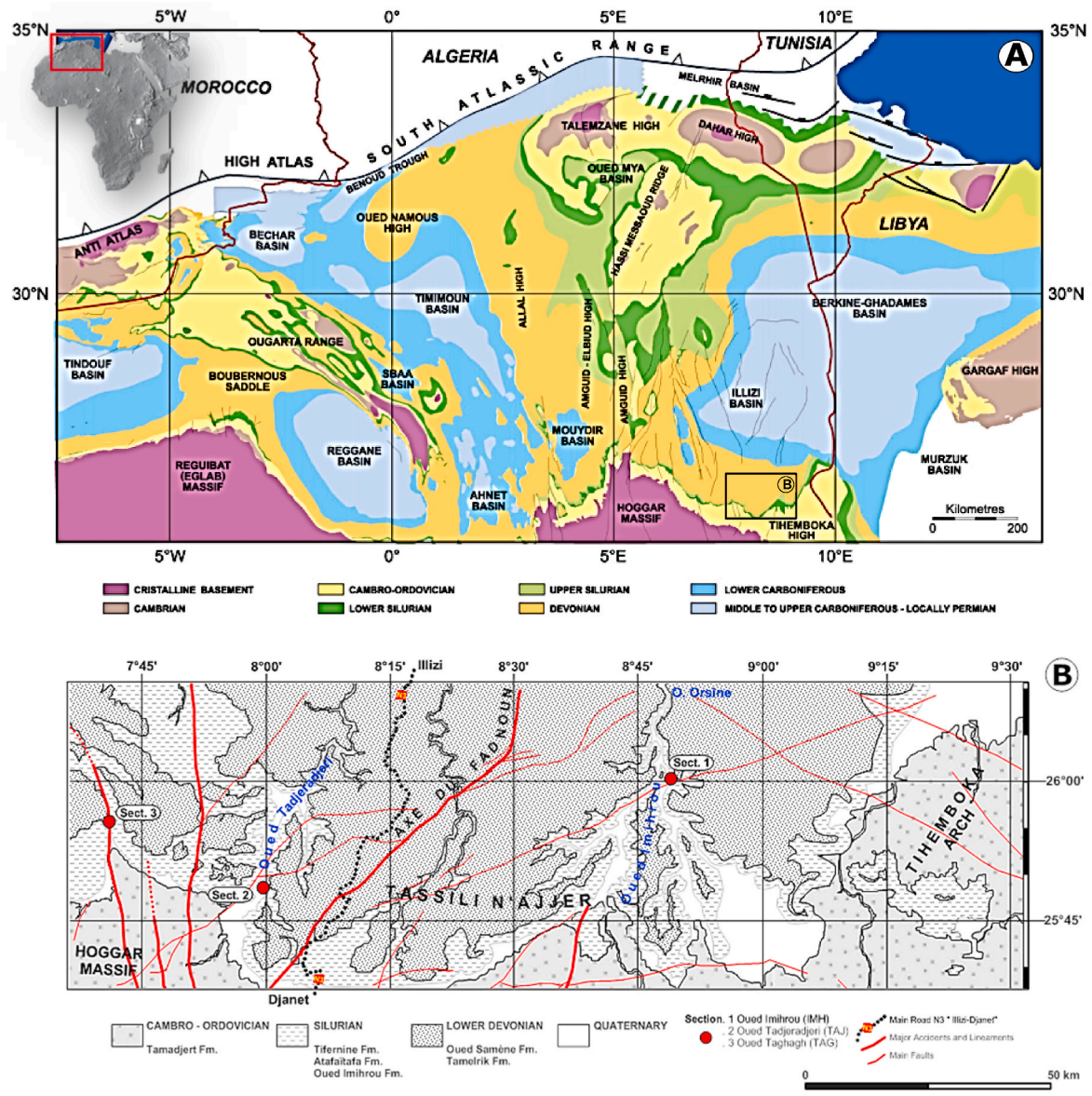

Fig. 1. (**A**) Pre-Mesozoic subcrop map of the Algerian Saharan Platform, showing the main Late Paleozoic (mostly 'Hercynian') – early Mesozoic tectonic elements and situation of the Berkine – Ghadames, and Illizi basins "BGI" (from Galeazzi et al., 2010). The rectangle corresponds to the Tassili n'Ajjer studied area. (**B**) Map showing the location of sedimentological sections in the Tassili n'Ajjer plateau (modified from the geological map of Illizi at the scale of 1:200,000 published by BeicipFranlab – IFP, and Sonatrach, 1974–1975, limited access).

Formation, and the Oued Tifernine Formation, which can be distinguished across the entire investigated area and laterally traceable over kilometers. The present work focuses on the two first formations of the Silurian in Algeria (Fig. 2). The Oued Imihrou Formation, about 130 m-thick succession of Llandovery in age, consists of shelfal organic-rich graptolite-yielding black shales and light grey-green laminated micaceous 'lean' shales, which are deposited during a large-scale synchronous anoxic event that is apparent across northern Gondwana and in shallow-marine storm-dominated shoreface environment, respectively. The Atafaïtafa Formation, 130 m-thick of late Llandovery to Wenlock, consists of an alternation of mudstone and non-bioturbated sandstone deposits, mainly of foreshore open-shoreline systems with deposition under tidal and oscillation processes during a regressive regime (Djouder et al., 2018).

A total of sixty-five representative samples were collected from a fresh material, i.e., well-preserved escarpment cliffs, to minimize the effects of weathering, and all have been characterized to investigate the continuous stratigraphic series of the Oued Imihrou Formation (Llandovery) and the Atafaïtafa Formation (late Llandovery to Wenlock). The three different sites were carefully selected from the Tassili n'Ajjer plateau in Algeria (Oued Imihrou, Tadjeradjeri, and Taghagh sections), and their location is reported in Figs. 1B and 2.

3. Analytical methods

3.1. X-ray diffraction

The whole rock of sixty-five samples were crushed gently, without grinding, to chips-size particles in preparation for separation of the clay-size fraction. Approximately 20–30 g of the bulk sample was disaggregated in 200 mL deionized water by stirring vigorously for 1–2 min without any chemical pre-treatment, following the procedures outlined by Moore and Reynolds (1997). Suspensions in beakers were placed in an ultrasonic bath for 2–3 min to ensure complete disaggregation. Deflocculation of clays was performed by successive washing with deionized water. The clay fraction of all samples (infra 2 μm particles)

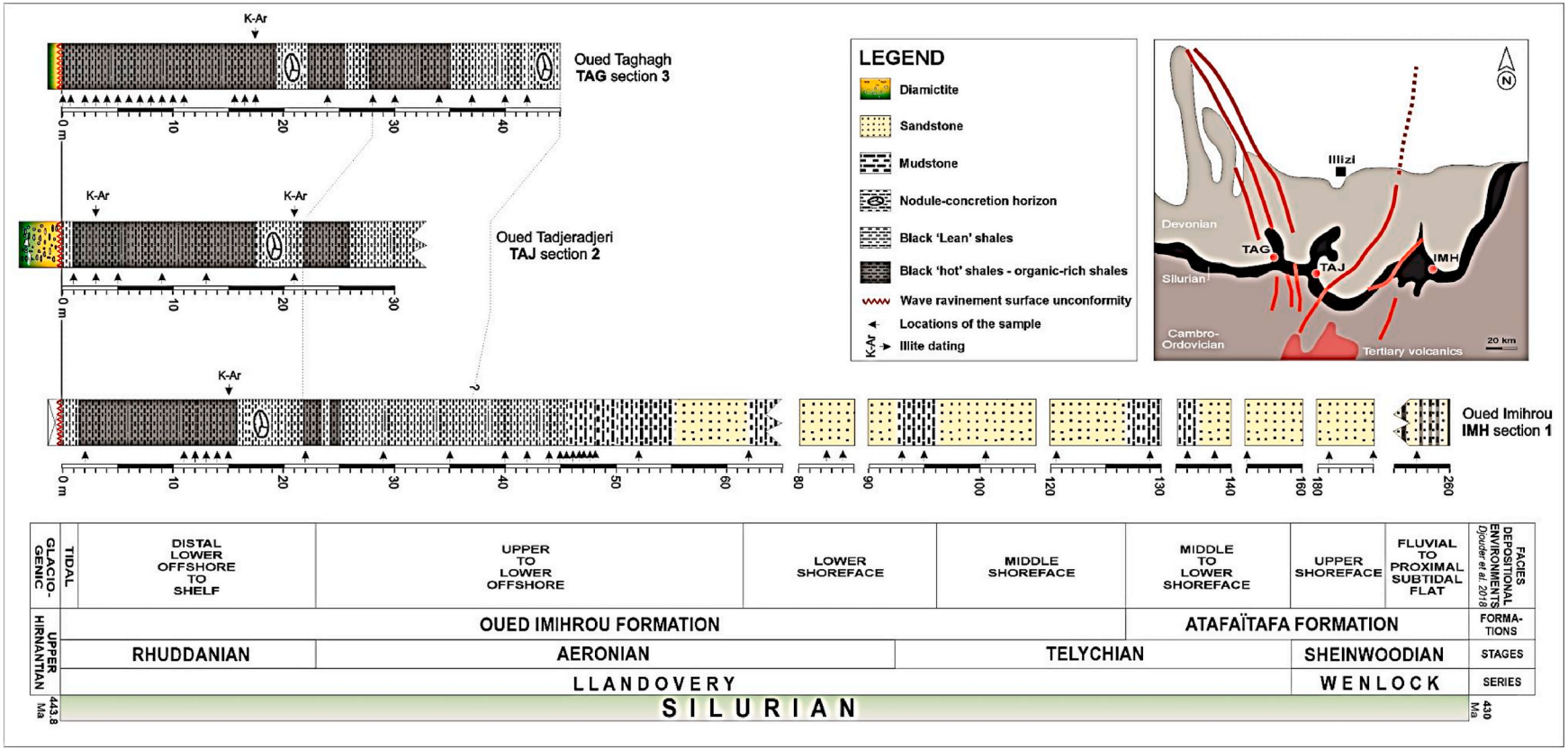

Fig. 2. Lithology, depositional environments, and location of the studied samples throughout the three Silurian outcrop sections from the Tassili n'Ajjer plateau (cf. Djouder et al., 2018).

Table 1
Clay fraction mineralogy, measured illite crystallinity, and intensity ratio of the studied samples from the eastern- and western-Tassili n'Ajjer plateau. ML: mixed layers, I/C: illite-chlorite, NCH*: nodule-concretion horizon. CIS-calibrated *IC*: [$IC_{Present\ work} = (0.7338 * IC_{CIS}) + 0.0372$].
++++ Dominant (>60%), +++ Major (20–60%), ++ Minor (up to 20%), + Trace (<5%), * Believed to be present.

Sample n°.	Outcrop Position (m)	Age	Clay Mineralogy Kaolinite	Illite	Chlorite	ML or I/C	Illite FWHM Crystallinity Present work "raw" IC (Δ°2θ)	CIS-calibrated IC (Δ°2θ)	Illite ratio Ir [(001)/(003)AD]/[(001)/(003)EG]
Eastern Tassili n'Ajjer									
Oued Imihrou IMH (section 1)									
ALT 1	2	Rhuddanian	+++	++			0.99	1.30	1.00
ALT 1b	11	Rhuddanian	+++	++		*	1.00	1.31	1.12
ALT 1d	12.5	Rhuddanian	+++	++		*	1.00	1.31	0.98
ALT 1e	13	Rhuddanian	+++	++			0.98	1.28	1.03
ALT 1f	14	Rhuddanian	+++	++			1.15	1.52	0.94
ALT 1g	15	Rhuddanian	+++	++			1.19	1.57	1.03
NCH*	19								
ALT 1h	22	Rhuddanian	+++	++			1.12	1.48	0.99
ALT 2a	29	Rhuddanian	+++	++		*	0.79	1.03	1.08
ALT 2b	35	Rhuddanian	+++	++	+	*	0.90	1.18	0.95
ALT 3-14	40	Rhuddanian	+++	++	+	*	1.00	1.31	0.92
ALT 3	42	Rhuddanian	+++	++			0.80	1.04	1.03
ALT 4	44	Rhuddanian	+++	+					1.08
ALT 6a	45	Rhuddanian	+++	++		*	0.89	1.16	1.04
ALT 6b	45.5	Rhuddanian	+++	++			1.20	1.58	1.02
ALT 7	46	Rhuddanian	+++	++	+		0.83	1.08	1.03
IMH 0	46.5	Aeronian	+++	++			0.49	0.62	1.08
IMH 1a	47	Aeronian	+++	++		*	0.93	1.22	*1.51*
IMH 2	47.5	Aeronian	+++	++		*	1.16	1.53	*1.49*
IMH 2a	48	Aeronian	+++	++	+		0.91	1.19	0.96
IMH 3	52	Aeronian	+++	++	+		0.70	0.90	1.11
IMH 9	62	Aeronian	+++	+	+	*	0.33	0.40	1.09
IMH 14c	82.5	Aeronian	+++	+	+		0.64	0.82	1.04
IMH 15	84	Aeronian	+++	+	+		0.46	0.58	1.00
IMH 15c	93	Telychian	+++	+	+		0.65	0.84	0.85
IMH 15d	95	Telychian	+++	+	+		0.65	0.84	0.98
IMH 16	100.5	Telychian	+++	+	+	*	0.68	0.88	*1.65*
IMH 21a	121	Telychian	+++	+	+		0.41	0.51	1.06
IMH 25	129	Telychian	+++	+			0.80	1.04	1.09
IMH 28	136	Telychian	+++	+			1.03	1.35	1.06
IMH 29b	138.5	Telychian	++++	+		*	0.84	1.09	1.03
IMH 30	155	Telychian	++++	+					
IMH 36	182	Sheinwoodian	++++	+					
IMH 37	185.5	Sheinwoodian	++++	+			0.50	0.63	0.97
IMH 59	255.5	Sheinwoodian	++++	+			0.55	0.70	1.05
Western Tassili n'Ajjer									
Oued Tadjeradjeri TAJ (section 2)									
InTaf 2	1	Rhuddanian	+++	++			0.60	0.77	1.05
TAJ 0	3	Rhuddanian	+++	++			1.00	1.31	1.09
TAJ 1	5	Rhuddanian	+++	++			0.70	0.90	1.04
TAJ 2	9	Rhuddanian	+++	++			1.07	1.41	1.10
TAJ 3	13	Rhuddanian	+++	++			1.13	1.19	1.02
NCH*	19								
TAJ 4	21	Rhuddanian	+++	++			0.88	1.15	1.07
Oued Taghagh TAG (section 3)									
TAG 1	0	Rhuddanian	+++	++	+		0.42	0.52	1.07
TAG 1a	0.5	Rhuddanian	+++	++	+		0.50	0.63	
TAG 1b	2	Rhuddanian	+++	++	+		0.60	0.77	0.96
TAG 1c	3	Rhuddanian	+++	++	+		0.51	0.64	0.94
TAG 1d	4	Rhuddanian	+++	++	+		0.56	0.71	0.99
TAG 1e	5	Rhuddanian	+++	++	+		0.54	0.69	0.99
TAG 2-16	6	Rhuddanian	+++	++	+		0.31	0.37	0.99
TAG 2a	7	Rhuddanian	+++	++	+		0.38	0.47	1.02
TAG 2b	8	Rhuddanian	+++	++	+		0.55	0.70	1.05
TAG 2c	9	Rhuddanian	+++	++	+		0.32	0.39	1.02
TAG 2d	10	Rhuddanian	+++	++	+		0.55	0.70	0.98
TAG 3-15	11	Rhuddanian	+++	++			0.93	1.22	1.08
TAG 3-16	15.5	Rhuddanian	+++	++			0.86	1.12	0.94
TAG 3a	16.5	Rhuddanian	+++	++	+		0.32	0.39	0.83
TAG 3b	17.5	Rhuddanian	+++	++	+		0.74	0.96	1.11
NCH*	21								
TAG 3d	24	Rhuddanian	+++	++	+		0.56	0.71	1.05
TAG 3d-15	28	Rhuddanian	+++	++			0.32	0.39	1.00
TAG 3e	30	Rhuddanian	+++	++	+		0.51	0.64	1.03
TAG 4	34	Rhuddanian	+++	++	+	*	0.77	1.00	0.95
TAG 4a	37	Rhuddanian	+++	++	+		0.51	0.64	0.99

(*continued on next page*)

Table 1 (*continued*)

TAG 4b	40	Rhuddanian	+++	++	+	0.68	0.88	1.16
TAG 4c	42	Rhuddanian	+++	++	+	0.40	0.49	1.05

and the submicron fraction of four selected samples (<0.2 and < 0.1 μm) were separated by MPW 350E centrifuge and a Sigma 3–16L ultra-centrifuge respectively.

The diffraction patterns were collected with a Bruker D4 Endeavor X-ray diffractometer fitted with a normal-focus Cobalt X-ray tube, Fe filter, and a Lynxeye position-sensitive detector at CSIRO, Australia. Clay sized oriented fractions were analyzed over the range of 2theta = 2–35° at 0.015° 2θ/s after successive air drying (AD), ethylene glycol (EG) saturation for 24 h, and heating treatment (H) to 550 °C during 2 h. The bulk powdered samples were examined between 5 and 90° 2θ angular ranges and minerals were quantified with Siroquant (program using the Rietveld method). Bruker's DIFFRAC.EVA software was used for background stripping, indexing of diffraction peaks, and identification of mineral phase by comparison with International Centre for Diffraction Data (ICDD) files.

3.2. The illite crystallinity and intensity ratio

Several methods have been proposed to quantify the crystallinity index of illite (*IC*) (see Frey, 1987; Abad, 2007). The most common indicator is the illite crystallinity index (otherwise named "Kübler index" Kübler and Jaboyedoff, 2000), defined as the full width at half maximum peak intensity (FWHM) of the first order illite basal reflection (10 Å peak in the AD preparation), and expressed as small changes in the Bragg angle, Δ° 2θ values (e.g. Kübler, 1967; Kübler and Jaboyedoff, 2000). Indeed, in clay mineralogy changes in the shape of the XRD 10 Å-illite peak are diagnostic of alterations in the grade diagenesis and incipient metamorphism (Kübler, 1968; Frey, 1987; Guggenheim et al., 2002; Meunier, 2005; Ferreiro Mählmann et al., 2012). In this study, illite crystallinity (*IC*) values were measured on samples of <2 μm fraction containing only insignificant amounts of expandable mixed-layers, as deduced from the small changes in intensity at the high-angle side of the 001 reflections after glycol treatment. Standard samples of Warr and Rice (1994) were used for calibration with respect to the Crystallinity Index Standard (CIS) approach (cf. Warr and Ferreiro Mählmann, 2015). As internationally accepted (Frey, 1987; Árkai, 1991), the following zones of the diagenetic/metamorphic grade and the illite crystallization degree are defined by Kübler-Index values with respect to the Kübler-Frey-Kisch calibration: *diagenetic zone* (low grade diagenesis) ≥1.0 Δ°2θ, (high grade diagenesis) 0.62–1.0 Δ°2θ and (highest grade diagenesis) 0.42–0.62 Δ°2θ; *anchizone* (low grade anchi-metamorphic) 0.33–0.42 Δ°2θ and (high grade anchi-metamorphic) 0.25–0.33 Δ°2θ; and *epizone* (epi-metamorphic grade) ≤0.25 Δ°2θ (Kübler, 1967; Kisch, 1987). While, for *IC* values determined using the recommended CIS calibration, the equivalent limits are slightly different: illite crystallization values of greater than 0.53 Δ°2θ indicate conditions of diagenesis; values of 0.36–0.53 Δ°2θ indicate anchizone, and values less than 0.36 Δ°2θ indicate metamorphic (epigenesis) conditions (see Ferreiro Mählmann et al., 2012; Warr and Ferreiro Mählmann, 2015). These three metamorphic zones roughly correspond to temperatures lower than 200 °C for the diagenetic zone, 200–300 °C for the anchizone, and above 300 °C for the epizone (Warr and Ferreiro Mählmann, 2015). However, the exact delimitation of the illite crystallinity boundary values in terms of metamorphic grade is equivocal at present (see Ferreiro Mählmann and Frey, 2012 and references therein). In view of this ongoing controversy, the present study followed the methodological recommendations of Kisch et al. (2004), and it provides both the CIS-calibrated and "raw" (as measured) *IC* values (Table 1). For simplicity, however, the term *IC* is retained further in the text and corresponds to the CIS-calibrated values.

The intensity ratio (*Ir*) was also measured during this study, using the *Ir* introduced by Środoń (1984): $Ir = [(001)/(003)_{air-dried}]/[(001)/(003)_{glycol}]$. The *Ir* denotes the intensity ratio of the 001 and 003 reflections from air-dry and glycolated samples. According to the same author, the positions, shapes and relative intensities of 00*l* reflections of an illitic material often change slightly after EG treatment, indicating some mixed-layering. Therefore, this ratio is very sensitive to the presence of swelling layers in illite or having very small expandabilities ($Ir > 1$) and a value of $Ir = 1 \pm 0.1$ is indicative of pure illite (Środoń, 1984, 2013).

3.3. Electron microscopy

The textural and spatial relationships of authigenic and detrital minerals including clays were examined from twenty clay separates and rock-chips at CSIRO. A field emission scanning electron microscope (ZEISS Ultra-*plus* FE-SEM) equipped with an EDS detector, was used for the back-scattered electron (BSE) imaging and energy-dispersive X-ray (EDX) analysis, operating at 5–15 kV accelerating volts, 1.5 nA beam current, and 5–16.5 mm working distance. The particle micromorphology was studied on carbon (clay <2 μm) and gold-coated rock-chips using the secondary electron mode (SE).

3.4. Organic petrography of graptolites

Thermal maturity parameters including differentiation of metamorphic subfacies, reflectance data, and whole rock programmed pyrolysis were determined on eleven Early Silurian organic-rich samples (Oued Imihrou Formation) selected from surface outcrops at three distinct locations (cf. Fig. 2).

There are many advantages to using vitrinite reflectance and it is generally considered to be the most useful thermal maturity index for post-Devonian rock sequences in hydrocarbon exploration (Hackley et al., 2015; Luo et al., 2020). However, for pre-Devonian argillaceous series such as those analyzed here, i.e., Silurian, graptolites are the most widely used zooclast group for reflectance measurements because the evolution of their optical properties is comparable to that of vitrinite (Teichmüller, 1958, 1986; Goodarzi and Norford, 1987, 1989; Taylor et al., 1998; Link et al., 1990; Petersen et al., 2013; Hartkopf-Fröder et al., 2015; Suchý et al., 2015). According to Petersen et al. (2013), measurements based on bitumen reflectance are less reliable for maturity determination, because bitumen may have various morphologies and origins, and it may not be indigenous to the host rock. In this study, all reflectance measurements for thermal maturity assessment were carried out mostly on graptolite fragments and "vitrinite"-like particles, which can be converted to vitrinite reflectance equivalents (VR_{eqv}).

The organic matter petrography and reflectance measurements were performed both on sections cut perpendicular and parallel to the plane of bedding, placed in a 30 mm diameter mold along with several randomly oriented grains, and set in a cold epoxy resin block. The epoxy resin-mounted samples were polished using a variety of wet and dry papers, diamond polishing compounds, and colloidal silica. The polished samples were dried in a desiccator for a minimum of 12 h prior to analysis at Energy Resources Consulting Pty Ltd, Australia. Graptolites and "vitrinite"-like particles reflectance were measured according to methods previously described in Hoffkecht (1991) and Goodarzi et al. (1992). A Leica MP4500P reflected light microscope equipped with monochromatic light (λ = 546 nm, 2 μm^2 area) source, a 50 × oil objective lens under oil immersion (refractive index, $n_e = 1.518$ at 23 °C), was used in accordance with the International Committee for Coal and Organic Petrology - ICCP (ISO 7404-3, 2009; ISO 7404-5, 2009). Plane polarized light was used and the microscope stage

Table 2
Vitrinite reflectance equivalents (VR_{eqv}) data of representative samples from the eastern- and western-Tassili n'Ajjer plateau. Reflectance measurements on graptolite, and on VLPs.

Sample n°.	Outcrop Position (m)	Age	Lithology	Maceral Types	Mean Birefl.	Graptolite Reflectance N	SD	Range Min. Max.		GR_{omax}	Vitrinite Reflectance Equivalent N	SD	Mean GR_{omax}	VR_{eqv}
Eastern Tassili n'Ajjer Oued Imihrou IMH (section 1)														
ALT 1	2	Rhuddanian	Calcareous claystone and carbonate	Graptolite	/	/	/	/	/	/	14	0.120	1.23	1.14
				"Vitrinite" like particles	/	14	0.120	1.02	1.45	1.23				
ALT 3	42	Rhuddanian	Fine claystone	Graptolite	/	/	/	/	/	/	25	0.143	1.22	1.13
				"Vitrinite" like particles	0.25	25	0.143	0.95	1.46	1.22				
IMH 0	46.5	Aeronian	Calcareous claystone and carbonate	Graptolite	/	/	/	/	/	/	16	0.147	1.27	1.16
				"Vitrinite" like particles	/	16	0.147	1.00	1.54	1.27				
Western Tassili n'Ajjer Oued Tadjeradjeri TAJ (section 2)														
InTaf 2	1	Rhuddanian	Silty claystone with thin bands of siltstone	Graptolite	0.74	14	0.070	1.51	1.78	1.62	39	0.159	1.62	1.34
				"Vitrinite" like particles	0.14	25	0.079	1.16	1.48	1.33				
TAJ 1	5	Rhuddanian	Silty claystone with abundant pyrite	?Graptolite	/	4	0.110	1.11	1.42	1.26	29	0.211	1.26	1.15
				"Vitrinite" like particles	/	25	0.086	0.53	0.91	0.70*				
TAJ 3	13	Rhuddanian	Silty claystone and argillaceous siltstone	Graptolite	/	/	/	/	/	/	6	0.134	1.14	1.09
				"Vitrinite" like particles	0.50	6	0.134	0.96	1.33	1.14				
Oued Taghagh TAG (section 3)														
TAG 3-15	11	Rhuddanian	Silty claystone	Graptolite	0.43	25	0.182	1.88	2.51	2.20	50	0.345	2.20	1.64
				"Vitrinite" like particles	0.10	25	0.099	1.38	1.79	1.57				
TAG 3-16	15.5	Rhuddanian	Silty claystone	Graptolite	0.39	25	0.190	1.92	2.58	2.21	50	0.446	2.21	1.64
				"Vitrinite" like particles	0.03	25	0.156	1.02	1.73	1.39				
TAG 3d-15	28	Rhuddanian	Fine claystone	Graptolite	0.53	25	0.098	1.50	1.88	1.68	50	0.236	1.68	1.37
				"Vitrinite" like particles	0.12	25	0.048	1.13	1.33	1.23				
TAG 4	34	Rhuddanian	Silty claystone with common pyrite	Graptolite	0.46	11	0.314	1.90	2.96	2.59	36	0.545	2.59	1.84
				"Vitrinite" like particles	0.07	25	0.167	1.17	1.85	1.51				

Abbreviations: Mean of all the maximum reflectance readings obtained (GRomax). The range minimum-maximum reflectance, i.e., the lowest GRomax and highest GRomax of the population considered to represent the first generation vitrinite population, the mean bireflectance, the number of fields measured N (Number of measurements = 2N because 2 maximum values are recorded for each field), and the standard deviation (SD). VReqv (Luo et al., 2020): [%VReqv = (0.515 * GRomax) + 0.506].

rotated 360° such that the mean of all the maximum reflectance ($GR_{o\text{-}max}$), the range minimum-maximum reflectance, i.e., the lowest GR_{omax} and highest GR_{omax} of the population considered to represent the first generation vitrinite population and mean bireflectance values could be obtained. Maximum reflectance values are preferred as the standard deviation (SD) of the mean is smaller compared to random reflectance values (GR_{or}), which is especially important at higher maturations and when the population size is small. In addition, mean bireflectance can be calculated which can give an indication of the importance of regional versus contact metamorphism.

Both minimum-maximum oil reflectances of the same individual organic fragments were measured by rotating the microscope stage, while a polarizer was placed in the incident light path, and the mean bireflectance [(mean max – mean min)/(mean max)] was calculated using polarized light. The number of reflectance measurements (N) varied from 6 to 50 measurements for every sample ($N_{average}$ = 30; Table 2). The most reliable method of assessing the level of thermal maturity of graptolites is the GR_{omax}, taken under polarized light, rather than the random reflectance GR_{or}. Because, even with a positive correlation between GR_{omax} and GR_{or} (Luo et al., 2020), GR_{omax} measurements always display a lower SD compared to random measurements of all the analyzed samples. Indeed, graptolites are anisotropic with biaxial optical properties and have extremely strong mean bireflectance at advanced maturity as pointed out by Link et al. (1990) and Goodarzi et al. (1992) elsewhere.

Vitrinite reflectance equivalent (VR_{eqv}) of each sample was obtained using the recent conversion equation of Luo et al. (2020): [$\%VR_{eqv} = (0.515 * GR_{omax}) + 0.506$].

Paleotemperature estimates for the graptolitic Early Silurian shales, through VR_{eqv}, were calculated using the linear regression equation of Barker and Pawlewicz (1986) and have an error of ±20 °C, [$\ln(R_m) = (0.0078 * T_{max}) - 1.2$]. In this study $\%R_m = VR_{eqv}$ and paleotemperatures T_{max} are in units of °C. This time-independent empirical method was chosen due to the limited influence of heating duration on thermal maxima recorded by organic material (Barker and Pawlewicz, 1986).

3.5. Programmed pyrolysis

Source rock analyses were conducted using the latest version of the Rock-Eval pyrolysis technique under the HAWK™ Instrument from Wildcat Technologies at Energy Resources Consulting Pty Ltd, Australia (e.g. Espitalié et al., 1985; Lafargue et al., 1998; Behar et al., 2001). The whole rock pyrolysis was used to estimate the hydrocarbon potential of eleven unweathered rock samples by open system volatilization and cracking of organic matter according to a programmed temperature pattern.

The pyrolyzed hydrocarbons are monitored by a flame ionization detector (FID) with the 'Institut Français du Pétrole' (IFP) standard rock,

Table 3
Programmed pyrolysis, derived parameters and their respective *IC*, VR_{eqv} and calculated temperatures of selected samples from the eastern- and western-Tassili n'Ajjer plateau. HI = (S2 X 100)/TOC; OI = (S3 X 100)/TOC; PI = S1/(S1 + S2). $T_{max(calculated)}$ (Jarvie et al., 2001; Laughrey, 2014): [%VR= (0.0180 * T_{max}) − 7.16]. Paleotemperature estimates (Barker and Pawlewicz, 1986): [ln(VR_{eqv}) = (0.0078 * T_{max}) – 1.2]. * Anomalous values.

Sample n°.	Outcrop Position (m)	Lithology	TOC (wt. %) Total Organic Carbon	Rock-Eval Pyrolysis & Derived Parameters HI Hydrogen Index	OI Classical Oxygen Index	S1 (mg/g) Free Oil	S2 (mg/g) Kerogen Yield	S3 (mg/g) S3CO2	OI-RE6 RE6 Oxygen Index	PI Production Index	S3' (mg/g)	S3CO (mg/g)	S3'CO (mg/g)	S4CO (mg/g)	S4CO2 (mg/g)	S5 (mg/g)	Al Adsorption Index	OSI Oil Sataturation Index	GOC Generative Organic Carbon	NGOC non-Generative Organic Carbon	Tmax (Rock-Eval) °C	Calculated Parameters Tmax (calculated) °C	VR_{eqv}	Paleo-temperature T °C
Eastern Tassili n'Ajjer Oued Imihrou IMH (section 1)																								
ALT 1	2	Black shale	0.11	36	73	0.02	0.04	0.08	323	0.33	1.87	0.17	0.21	2.13	0.01	0.33	0.09	18.18	0.02	0.09	456	461	1.14	171
ALT 3	42	Black shale	2.13	9	66	0.02	0.20	1.41	84	0.10	3.86	0.19	0.38	6.08	65.85	1.15	1.75	0.94	0.07	2.06	470	461	1.13	170
IMH 0	46.5	Black shale	0.14	29	71	0.07	0.04	0.10	182	0.64*	0.51	0.11	0.09	0.56	3.55	0.82	0.11	50.00	0.02	0.12	458	462	1.16	173
IMH 25	129	Siltstone	0.10	/	260	0.00	0.00	0.26	485	/	0.52	0.17	0.11	1.92	0.02	0.07	0.08	/	0.02	0.08	/	/	n/a	/
Western Tassili n'Ajjer Oued Tadjeradjeri TAJ (section 2)																								
InTaf 2	1	Black shale	0.73	23	33	0.13	0.17	0.24	77	0.43	1.32	0.20	0.24	3.56	19.37	0.80	0.60	17.81	0.05	0.68	351*	472	1.34	191
TAJ 1	5	Black shale	0.56	59	16	0.38	0.33	0.09	50	0.54*	1.06	0.15	0.08	3.78	11.96	0.53	0.46	67.86	0.07	0.49	434*	462	1.15	172
TAJ 3	13	Black shale	0.18	17	106	0.01	0.03	0.19	236	0.25	2.24	0.14	0.19	2.19	2.45	0.74	0.15	5.56	0.02	0.16	461	458	1.09	165
Oued Taghagh TAG (section 3)																								
TAG 3-15	11	Black shale	1.47	5	15	0.08	0.08	0.22	34	0.50	1.43	0.13	0.31	8.57	39.35	0.56	1.21	5.44	0.03	1.44	492	489	1.64	217
TAG 3-16	15.5	Black shale	1.48	6	16	0.03	0.09	0.23	43	0.25	1.68	0.22	0.36	8.73	39.56	0.54	1.22	2.01	0.03	1.45	470	489	1.64	217
TAG 3d-15	28	Black shale	2.09	20	29	0.22	0.41	0.60	49	0.35	2.36	0.22	0.42	8.14	60.52	1.25	1.71	10.53	0.09	2.00	437*	474	1.37	194
TAG 4	34	Black shale	0.48	81	25	0.05	0.39	0.12	64	0.11	0.84	0.12	0.13	3.42	10.42	0.48	0.39	10.42	0.05	0.43	347*	500	1.84	232

Table 4
Illite K–Ar geochronology results showing at least two generations of authigenic micrometric illite-type crystals: Oldest illite at about 335 Ma and youngest illite between 238 and 179 Ma.

Sample n°.	OutcropPosition (m)	Lithology	Grain size (μm)	K (%)	Rad.^{40}Ar (10^{-9} mol/g)	Rad.^{40}Ar (%)	K–Ar age ± 2σ (Ma)	Timescale: Period-Epoch-Stage
CSIRO* ID LP6-154				8.37	1.913	97.52	127.2 ± 1.8	Early Cretaceous-Barremian
GLO-174				6.55	1.112	95.20	95.3 ± 1.4	Late Cretaceous-Cenomanian
HD-B1-140				7.96	0.338	92.39	24.3 ± 0.3	Paleogene-Oligocene-Chattian
Eastern Tassili n'Ajjer Oued Imihrou IMH (section 1)								
ALT 1g	15	Black shale	<0.1	0.44	0.166	18.88	204.1 ± 6.2	Late Triassic-Norian
Western Tassili n'Ajjer Oued Tadjeradjeri TAJ (section 2)								
TAJ 0	3	Black shale	<0.2	2.29	1.465	52.98	335.5 ± 8.0	Carboniferous-Middle Mississippian-Visean
TAJ 4	21	Black shale	<0.2	1.43	0.467	47.78	179.2 ± 4.3	Lower Jurassic (Lias)-Toarcian
Oued Taghagh TAG (section 3)								
TAG 3b	17.5	Black shale	<0.1	0.19	0.084	15.01	238.3 ± 11.4	Middle Triassic-Anisian

forming the so-called peaks S_1 (thermovaporized free hydrocarbons thermally extracted at 300 °C), S_2 (pyrolysis products from cracking of organic matter up to 550 °C), S_3 (CO_2 released during the pyrolysis at higher temperatures) (Peters and Cassa, 1994). In addition, other parameters were automatically calculated, such as the total organic carbon (TOC, wt.%) content, $T_{max(Rock\text{-}Eval)}$ (temperature of the maximum yield of hydrocarbons S_2 peak), together with the *PI* (production index) and *HI* (hydrogen index). Due to the very low S_2 values and degree of thermal maturation, the analyses were carried out on 250 mg of a crushed sample rather than the standard 70 mg and pyrolysis up to a maximum temperature of 750 °C. In addition, all FID traces were manually examined and in a number of cases the machine determined $T_{max(Rock\text{-}Eval)}$ value was rejected in favor of a different, but lower, peak which was thought to better represent the thermal maturation. In some cases, alternative peaks were not available and the machine determined $T_{max(Rock\text{-}Eval)}$ value reported but may be unreliable. All the results are presented in Table 3.

3.6. K–Ar age dating

Authigenic, or newly formed illite and illite-type minerals, contain potassium and is, therefore, suitable for age determination using the potassium/argon (K/Ar) geochronometer (see the review from Clauer and Chaudhuri, 1995; Meunier and Velde, 2004). The radiometric K–Ar age of illite is useful, as this mineral often forms prior to hydrocarbon charge in response to heating in the same temperature range as oil formation (Dalrymple and Lanphere, 1969; Pevear, 1999; Hamilton, 2003).

Clay minerals of four size sub-fractions were prepared, separated using the high-speed Sigma 3–16L centrifuge as described in Uysal et al. (2000), and dated by conventional K–Ar age dating at the CSIRO Argon Laboratory (Australia). These size sub-fractions were extracted from selected representative samples after recording the XRD patterns of the <2 μm fraction, in order to reduce any contribution of the coarse detrital phyllosilicates (e.g. K-bearing phases), more importantly, to enrich and purify illite (Środoń et al., 2002; Franks and Zwingmann, 2010).

The K–Ar illite age analysis was completed on sub-fractions (<0.2 and < 0.1 μm) of four representative samples, which were collected from IMH section 1 (ALT-1g), TAJ section 2 (TAJ-0 and TAJ-4) and TAG section 3 (TAG-3b-15), following a procedure similar to that described by Bonhomme et al. (1975). At least 25 mg of sample material is required for $^{40}K/^{40}Ar$ analyses (Zwingmann et al., 2011). The potassium of each sample and standard was measured by ICP-OES, with an accuracy of better than 1% and each measurement was duplicated. For argon isotopic determinations, the samples were preheated under vacuum for at least 12 h at 80 °C to remove absorbed argon of atmospheric origin. Argon was extracted from the separated mineral fractions by fusing the samples within a vacuum line serviced by an on-line ^{38}Ar spike pipette. The isotopic composition of the spiked argon was measured with a high-sensitivity on-line VG3600 mass spectrometer using a Faraday cup. The ^{38}Ar spike was calibrated against HD-B1 standard biotite, and several international age standards were analyzed (cf. Odin et al., 1982; Hess and Lippolt, 1994). Blanks for the extraction line and mass spectrometer were systematically measured, and the mass discrimination factor was determined periodically by airshots. The error for argon analyses is below 2%, and the average $^{40}Ar/^{36}Ar$ value of the air measurements (AS134-AirS-1) yielded 295.81 ± 0.14, which is close to the recommended values of 298.6 ± 0.4 for the atmospheric $^{40}Ar/^{36}Ar$ ratio (Lee et al., 2006). Ages were calculated using the ^{40}K abundance and the decay constants of Steiger and Jäger (1977). The K–Ar age uncertainties consider the errors during sample weighing, K contents, $^{38}Ar/^{39}Ar$, and $^{40}Ar/^{38}Ar$ measurements and are quoted in the text as ± 2σ. Results are summarized in Table 4.

4. Results

4.1. Mineralogy

Clay mineralogy characterization, the measurements of illite crystallinity (*IC*), and intensity ratio (*Ir*) on the clay fraction (<2 μm) were measured for each sample and presented in Table 1. The sixty-five representative samples contain abundant graptolite particles, clay minerals and non-clay minerals such as quartz, muscovite, pyrite and minor phases: K-feldspar, iron oxides and carbonate. Moreover, important differences in mineralogy seem to be controlled by the lithology of the host rocks, stratigraphical level, and the paleogeographical location of the studied Silurian outcrop sections from the eastern- and western-Tassili n'Ajjer plateau.

The identified clay minerals include kaolinite (20–100%), mica-illite (0–20%), and chlorite (0–5%). In the eastern Tassili n'Ajjer plateau (IMH section 1), there is an increasing amount of kaolinite from the bottom (Oued Imihrou Formation) to the top of the section (Atafaïtafa Formation) and a decreasing trend of illite proportion (Fig. 3). Traces of chlorite (5%) are present in some samples from the IMH section and the

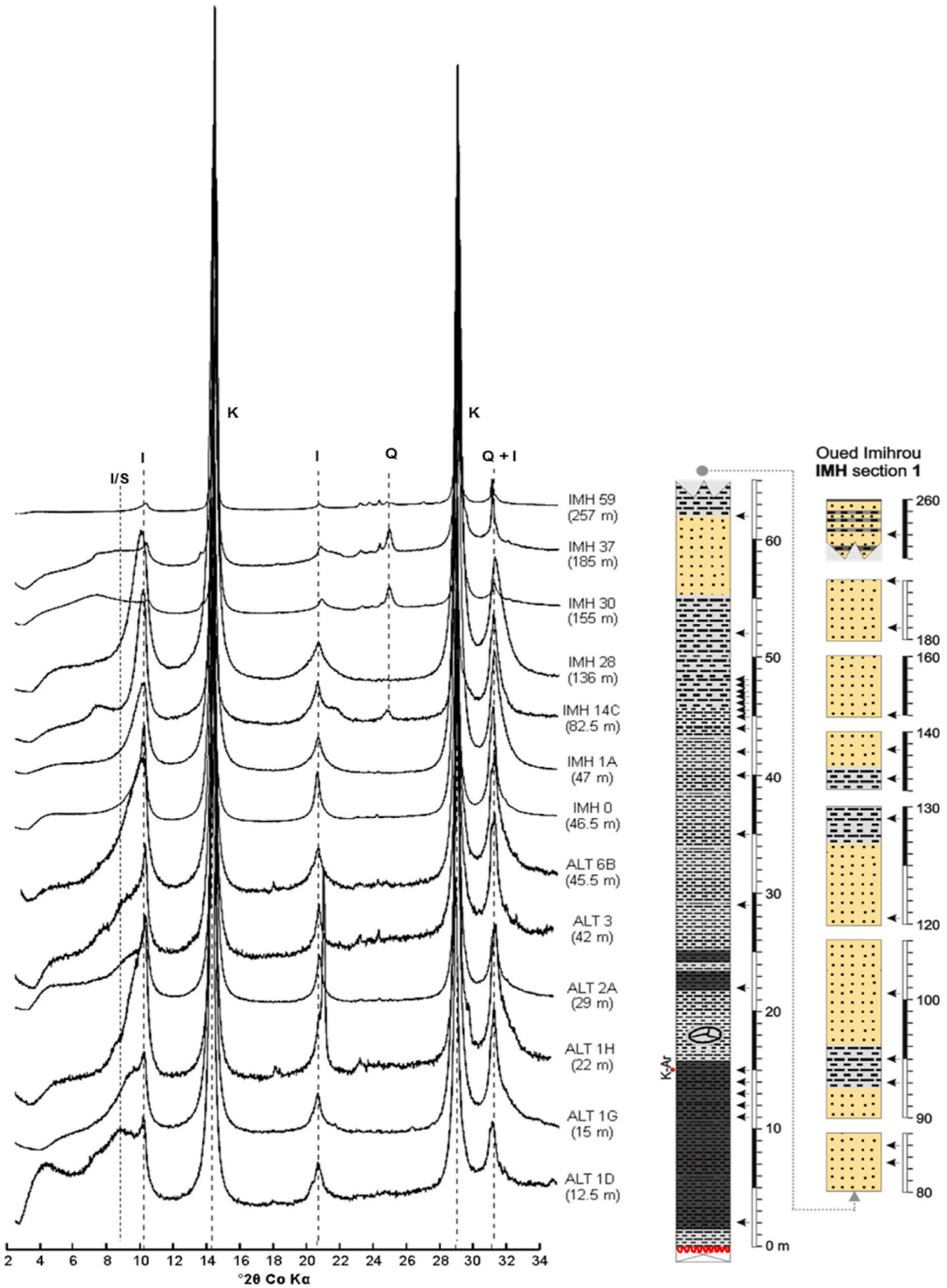

Fig. 3. Representative X-ray diffraction patterns of oriented preparations in <2 μm clay fractions (air-dried) from the Oued Imihrou Formation black shales and the overlying Atafaïtafa Formation sandstones, IMH section 1. (I/S: illite-smectite mixed layers, I: illite, K: kaolinite, and Q: quartz).

westernmost part of the Tassili n'Ajjer (TAG section 3), while a smectite phase is only present with a few percent as random mixed-layers (Table 1).

In this study, the CIS-calibrated *IC* (FWHM) index values, of all the studied samples, range widely from 0.37 to 1.58 $\Delta°2\theta$ (median = 0.90 $\Delta°2\theta$, n = 59; Table 1), following the calibration equation employed herein [$IC_{Present\ work} = (0.7338 * IC_{CIS}) + 0.0372$], $R^2 = 0.99$. These *IC* values cover the whole range of crystallization degrees from diagenetic

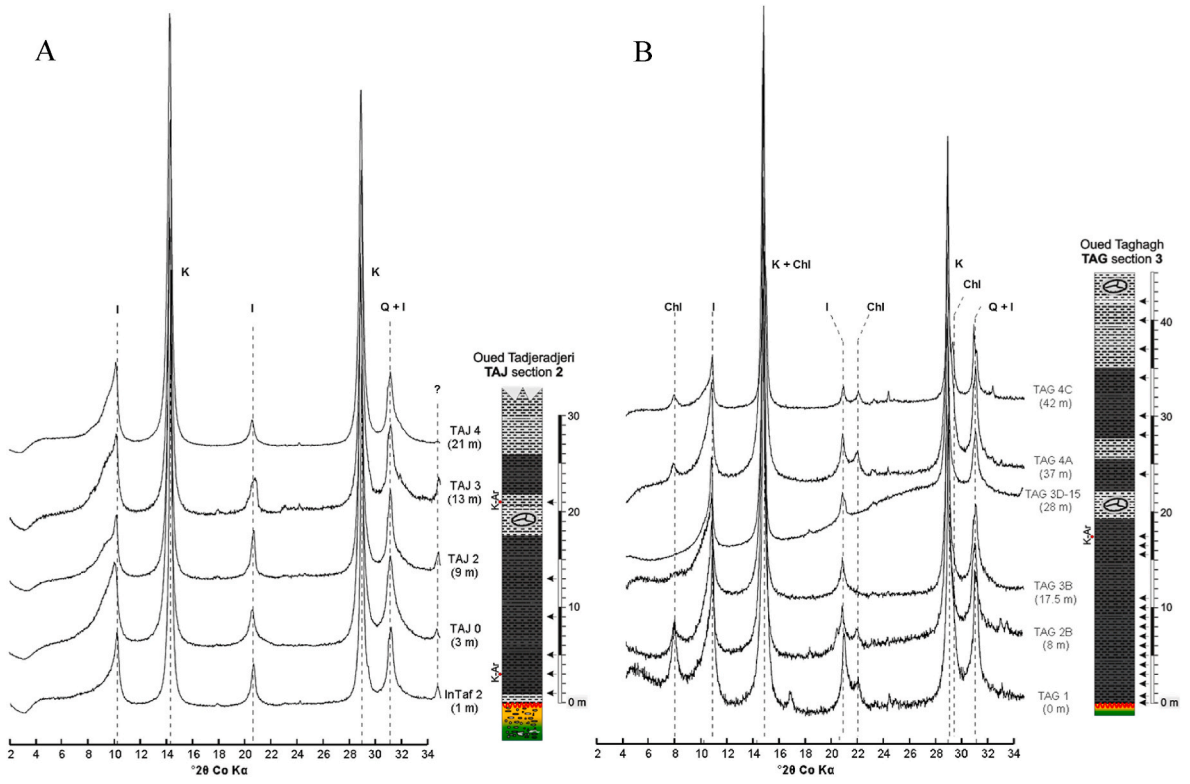

Fig. 4. Representative X-ray diffraction patterns of oriented preparations in <2 μm clay fractions (air-dried) from the Oued Imihrou Formation black shales, (**A**) TAJ section 2, and (**B**) TAG section 3. (I: illite, Chl: chlorite, K: kaolinite, and Q: quartz).

to incipient anchi-metamorphism intensity (e.g. Kübler, 1967; Kisch, 1987). Some samples from the extreme western Tassili n'Ajjer (TAG section 3) display *IC* values around or lower than 0.53 Δ°2θ, and indicating local higher temperature conditions than in the two other sections of the study area. Alternatively, these samples may have reached the upper anchizone to lower epizone. The *IC* values do not show a systematic decrease with stratigraphic age (outcrop position) but rather irregular distribution, which is reasonable as the most complete IMH section does not exceed 200 m in thickness.

Illite polytypism was not seen in the randomly oriented powder diffraction pattern of most samples from the study area, except for the four K–Ar prepared samples. The intensity ratio clusters around *Ir* values between 0.83 and 1.65 (median = 1.03, n = 59), indicating largely pure illite, and a very low amount of expandable components (≤5%) for the highest *Ir* values when mixed-layers could be present (e.g. Eberl and Velde, 1989; Środoń, 2013).

4.1.1. The western Tassili n'Ajjer plateau

Clay separates from the western- (TAJ) and the extreme western-part (TAG) of Tassili n'Ajjer consists of kaolinite (20–60%) and illite (up to 20%), while chlorite (<5%) is only present in TAG samples and completely absent within the TAJ samples. In those samples, the distinction between kaolinite and chlorite was based on observing the 002 peak of kaolinite at 3.58 Å and 004 peak of chlorite at 3.53 Å (Fig. 4B). Further, heating the samples at 550 °C for 2 h results in the complete destruction of kaolinite and an increase of the 001 reflection of chlorite with a slight contraction to about 13.9 Å, and thus confirms the presence of chlorite within the black shales and mudstones of TAG (Moore and Reynolds, 1997). In addition, the even-ordered (7.15 Å and 3.53 Å) peaks are more intense than the odd-ordered (14.2 Å and 4.71 Å) peaks, which is characteristic of iron-rich chlorite or chamosite (Brindley and Brown, 1980; Moore and Reynolds, 1997).

Illite is identified in XRD patterns by a series of peaks at about 10, 5 and 3.3 Å and present in all the samples. There is no significant change in either the peak positions or peak profile of 001 reflection of illites after glycolation and heating, thus confirming the possible absence of expandable smectite layers in the TAG- and TAJ illites. This was further confirmed for both sections by the *Ir* values of the (001) and (003) reflections; with values between 0.83 and 1.16 (median = 1.02, n = 27) according to a procedure described by Środoń (1984).

The TAG black shale samples contain 2*M* illite polytype, as identified in randomly oriented powders by the diagnostic non-basal lines at 4.09 Å, 3.88 Å, 3.72 Å, 3.20 Å, 2.98 Å, 2.86 Å, and 2.79 Å (Bailey, 1984). In contrast, both 2*M* and 1*M* illite (3.07 Å and 3.66 Å) polytypes coexist in TAJ samples. According to Dong et al. (1997), the increased dominance of $2M_1$ illite directly influences crystal thickening and hence *IC*. Indeed, as mentioned before, the TAG section yielded the lowest of all the measured CIS-calibrated *IC* values, ca. 0.37 Δ°2θ, with a median of 0.65 Δ°2θ (Table 1). These few low values point to the transition from the highest grade diagenetic conditions to the anchi-metamorphic illite crystallization degree, with a minimum temperature of 200 °C (Mullis et al., 1993; Warr and Ferreiro Mählmann, 2015 and references therein). These conditions could also explain the only occurrence of iron-rich chlorite and 2*M* illite with increasing temperature during diagenesis and very low-grade metamorphism, following the evolution of illite to muscovite of Hunziker et al. (1986) and the $1M$–$2M_1$ polytypic conversion of Frey (1987), Yang and Hesse (1991).

4.1.2. The eastern Tassili n'Ajjer plateau

The most complete section is located in the eastern Tassili n'Ajjer (IMH section 1) encompassing the Oued Imihrou Formation at the base (black 'hot' shales) and the overlying Atafaïtafa Formation (mudstones-sandstones). Kaolinite and illite are ubiquitous within the black shales, while the mudstones-sandstones alternations are characterized by kaolinite at the expense of illite, forming 60–100% of the clay fractions, as well as traces of other non-expandable clays (illite and chlorite) and only a small amount of expandable layers (Table 1 and Fig. 3). The latter are probably present within a few percent, as testified by the composed

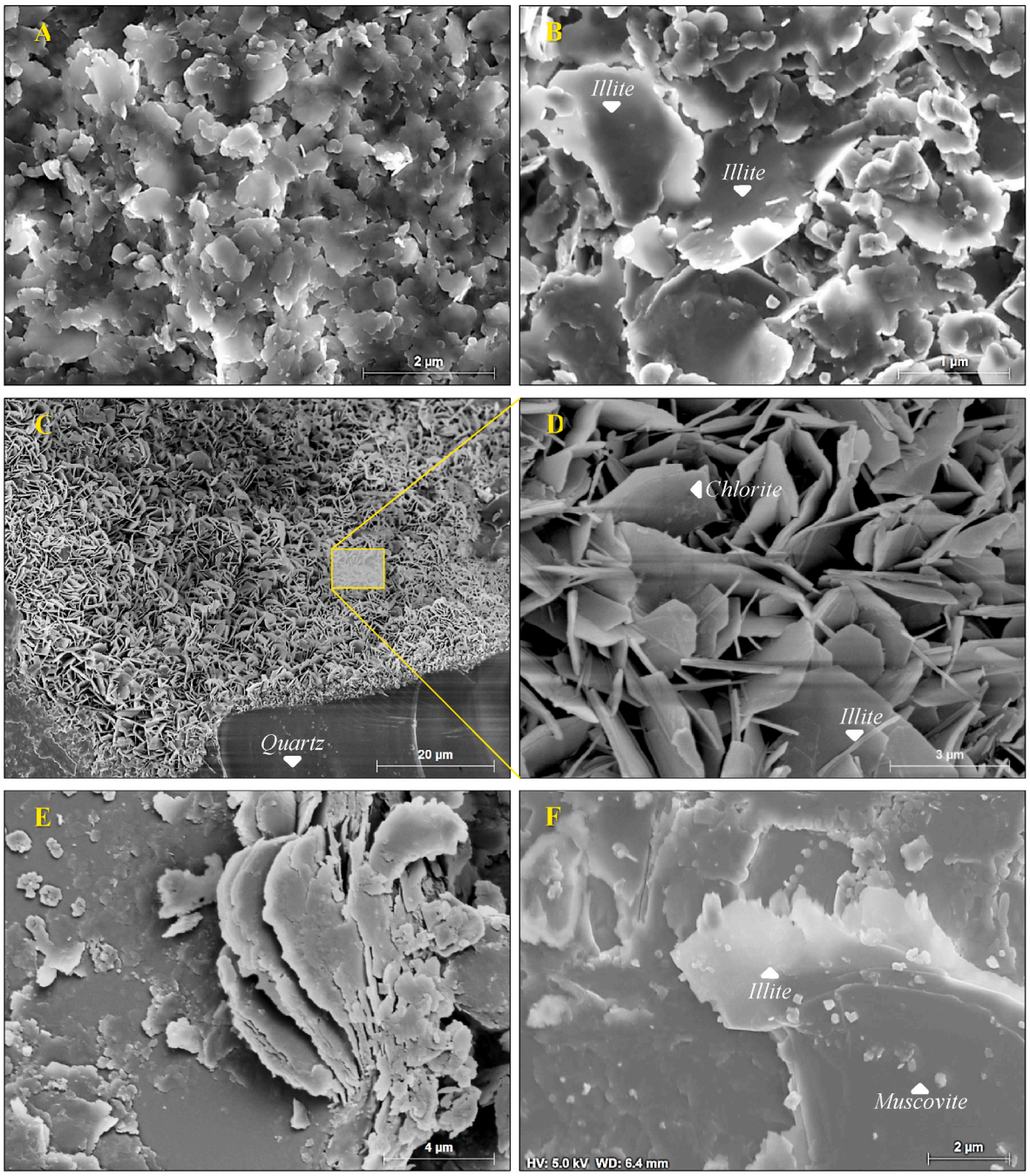

Fig. 5. SEM microphotographs of representative samples from the Oued Imihrou Formation shales and the Atafaïtafa Formation sandstones. A and B are clay fractions <2 µm, while C to F are bulk rock-chips. (**A**) *In situ* neocrystallization of illite minerals with platy shape reasonably close to hexagon platelets, sample IMH 0. (**B**) Overgrowth on the illite flakes, ALT 1. (**C**) Thick euhedral-crystallized iron-rich chlorite rims occurring as perpendicular rosettes, and coating detrital quartz grains, IMH 35. (**D**) Edge-to-face well-formed crystals of chlorite rims. Note the occurrence of sub-micrometer fiber 'hairy' illites that coexist and intergrow with chlorite. (**E**) Exfoliated muscovite showing a fan-shaped structure, TAJ 4. (**F**) Overgrowth of authigenic illite crystals on the basal surfaces of detrital muscovite, ALT 1g.

peaks with broad asymmetrical shapes and highest *Ir* values (~1.50). The CIS-calibrated IC values of the IMH section are shown to be the highest in comparison to the two other sections (median = 1.09 $\Delta°2\theta$, n = 31). In addition, *IC* values from the black shales, with only traces of 2*M* polytype, are much more coherent and expressed by values above 1 $\Delta°2\theta$, which broadly indicate diagenetic conditions (low-grade diagenesis).

4.2. Petrography of illitic clays

At least two populations of illite were distinguished by detailed SEM observations within the Oued Imihrou Formation shales and the Atafaïtafa Formation sandstones throughout the three studied Silurian outcrop sections. The black shale samples contain equant illite flakes with crystal shapes of near hexagonal platelets (Fig. 5A–B), while the porous sandstone samples display elongated fine-grained shapes (sub-micrometer) or fibrous 'hairy' illites, which usually coexist and intergrow with other phases like iron-rich chlorite (Fig. 5C–D). It is also

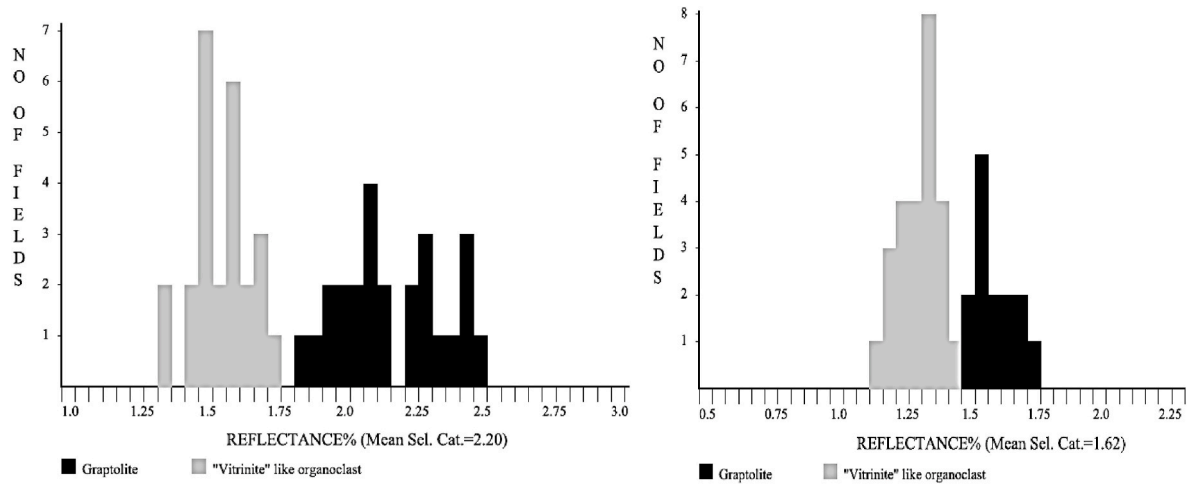

Fig. 6. Reflectance histograms show global bimodal distributions, thus suggesting the presence of two principal maceral populations: graptolite and "vitrinite"-like particles (Left: TAG 3–15 sample, Right: InTaf 2 sample).

important to note that some detrital muscovite crystals are exfoliated and their edges are fringed by the overgrowth of well-neocrystallized illite (<2 μm scale) confirmed by EDS analysis (Fig. 5E–F). Therefore, the shapes and morphologies of all of these illitic clays, at all observation scales, point to authigenic rather than detrital origin.

4.3. The reflectance of graptolites and source rock maturity

The examined zooclast and dispersed organic matter in eleven samples are judged indigenous to the host rock as they are oriented parallel within the bedding and with complete biological structures. They are commonly filled by abundant pyrite framboids confirming that the sedimentary organic matter was deposited and preserved under strongly reducing conditions (Djouder et al., 2018).

Reflectance histograms show globally bimodal distributions, thus suggesting the presence of two principal maceral populations: graptolites and "vitrinite"-like particles (Fig. 6). "Vitrinite"-like particles (VLPs) reported by Petersen et al. (2013) had a similar reflectance range to the associated graptolites and were suggested by them to be fragments of graptolites. However, in our study, VLPs have substantially higher reflectance and lower mean bireflectance (Table 2) than the associated graptolites. Especially, the lower mean bireflectance with the rare lamalginite, and liptodetrinite, displaying dull orange to weak brown fluorescence and which are commonly associated with degraded microplankton, suggest an algal origin of the VLPs in these samples. Indeed, the optical properties of algae, notably reflectance and fluorescence, change at a more rapid rate than that of associated vitrinites (when vitrinite is present) and presumably more rapidly than associated graptolites. It would therefore be expected that as maturation increases the reflectance values of algae would be initially lower, then equal and finally exceed that of the associated graptolites.

Graptolites were the most abundant organic remains in the Silurian shales (Llandovery) in North Africa, the Middle East and East Asia (Lüning et al., 2000; İnan et al., 2016; Luo et al., 2016). These fossil graptolites or rhabdosomes are macroscopically visible and easily identified both in polished blocks and reflected light microscopy; firstly, due to their characteristic internal and external morphology and, secondly, these graptolites have strong anisotropy, which increases with higher thermal maturity levels (Hartkopf-Fröder et al., 2015). The abundant zooclasts are of the non-granular fragments type (sensu Goodarzi, 1984). They display a wide range of shapes – elongated larger pieces (~0.05–2 mm long), irregularly lath-shaped lenses, angular or rounded, and occasional remnants of thecae with an intact periderm where both fusellar and cortical tissues are seen (Fig. 7A–D). In contrast, VLPs are lacking the diagnostic graptolite features and exhibit a more varied morphology. They occur as narrow strands and blocky particles orientated parallel to bedding and always occur in association with a thin band of diffuse organic matter (Fig. 7E–H). VLPs in the analyzed Lower Paleozoic shales are likely derived from slightly degraded algae and could be a type of coalified alginite. Additionally, mean bireflectance measurements are reliable on graptolites, however, no appreciable mean bireflectance was observed in VLPs as usually, the grain size is too small to make any reliable measurements.

The maturity of graptolitic Silurian sediments (Oued Imihrou Formation) from the three studied outcrop sections were evaluated by the mean maximum reflectances of graptolites- and VLPs. Their optical properties follow similar trends with increasing maturation to those of vitrinite, bitumen and chitinozoa, indicating similar molecular changes (Goodarzi, 1984; Goodarzi and Norford, 1987; Link et al., 1990). Therefore, all the reflectance measurements reported in this paper were carried out on these organic particles (Table 2). Nevertheless, it is obvious that the VR_{eqv} values of the IMH section, which are calculated only from VLPs in the lack of graptolite fragments, must be considered as much less reliable than the other values of the TAJ and TAG sections.

The measured GR_{omax} reflectance values show a great scatter, ranging from 1.14% to 2.59% (N = 315) with SD ranging from 0.048 to 0.314% ($SD_{average}$ = 0.134; Table 2). They also correspond to 1.09% and 1.84% VR_{eqv} of vitrinite reflectance equivalent, using the recent method of Luo et al. (2020). Such determined values indicate that the organic maturity corresponds to hydrocarbon generation zones that span from the oil generation phase through to condensate and wet gas, to the dry gas generation phase (e.g. Teichmüller, 1987; Mukhopadhyay, 1994). The corresponding very low S_2 values combined with $T_{max(Rock\text{-}Eval)}$ values above 430 °C (Table 3) are typical of such a maturity stage. In addition, the cross-plot of Hydrogen Index (HI) versus $T_{max(calculated)}$, or the Van Krevelen plot (Fig. 8), shows the maturity and the distribution of sedimentary organic matter types, which mainly contain kerogen Type II but behave like Type III. This is due to the high content of mature graptolites which are hydrogen-poor, and the predominantly aromatic groups and rings, with a lesser amount of aliphatic and carbonyl/carboxyl groups of the graptolite periderm, as discussed by İnan et al. (2016) and Morga (2020). In contrast, the immature graptolites are relatively hydrogen-rich, mainly gas prone, and have a significant hydrocarbon generation potential (Luo et al., 2020). It is apparent that samples from the eastern- (IMH section 1) and the western-Tassili n'Ajjer (TAJ section 2) show the lowest VR_{eqv} (median = 1.15, N = 129), largely of the late mature stage (oil window), ranging from 1.13–1.16% to 1.09–1.34%, respectively. In contrast, samples from the

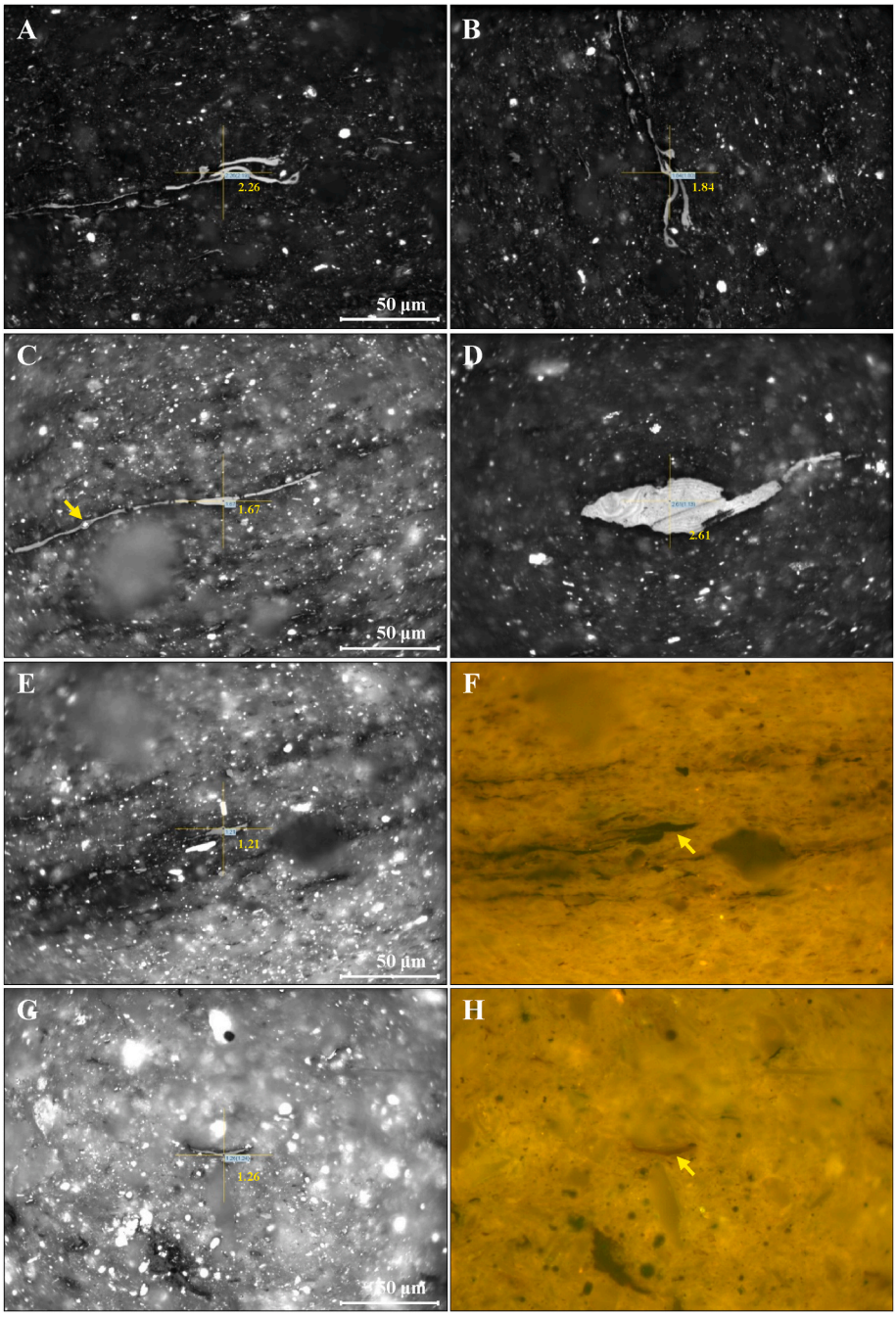

Fig. 7. Graptolites reflectance on well preserved non-granular large fragments and "vitrinite"-like particles (VLPs) reflectance. All photomicrographs are taken under white light with oil immersion objective 50 ×, note the anisotropy after rotating the stage at 90°. (**A**) Moderately bireflecting graptolite in silty claystone, GR_{omax} = 2.26%, reflected white light, TAG 3–15 sample. (**B**) Same grain, after rotating stage at 90° = 1.84%. (**C**) Strongly bireflecting graptolite, GR_{omax} = 1.67%, reflected white light, InTaf 2 sample. The arrow shows pyrite that fills the cavity of the rhabdosome. (**D**) Surface section of a non-granular graptolite periderm, showing fusellar layers and complex morphology, GR_{omax} = 2.61%, reflected white light, TAG 4 sample. The VLPs occur as narrow strands and blocky particles orientated parallel to bedding and are always occur in association with diffuse organic matter. (**E**) Weakly bireflecting VLPs in claystone, GR_{omax} = 1.21%, reflected white light, InTaf 2 sample. (**F**) Same grain, weak orange in fluorescence mode, showing clearly thin band of diffuse organic matter. (**G**) VLPs with rare lamalginite and liptodetrinite in silty claystone, GR_{omax} = 1.26%, reflected white light, TAJ 1 sample. (**H**) Same sample, dull orange to weak brown in fluorescence mode suggesting a maturation level of about 0.90% VR_{eqv}. (For interpretation of the references to colour in this figure legend, the reader is referred to the Web version of this article.)

westernmost part of the Tassili n'Ajjer (TAG section 3) display the highest VR_{eqv} values 1.37–1.84% (median = 1.64, N = 186) with a mean GR_{omax} that reaches 2.59%, and strong mean bireflectance of graptolite with increasing maturity. These values indicate that the sedimentary organic matter of TAG black shales broadly reached the advanced catagenesis to metagenesis stage, therefore, corresponding to lower wet and dry gas (methane) zones, specifically near the deep diagenetic-low anchizone boundary. This lower limit is correlated with VR values of 2.0–2.4% VR (i.e. CIS-calibrated *IC* values of ~0.53–0.4 $\Delta°2\theta$), and temperatures between 205 and > 265 °C (Mullis et al., 1993; Merriman and Frey, 1999; Ferreiro Mählmann and Frey, 2012). In this context, the obtained results from the organic petrography of graptolites show an excellent agreement and strong correlation with the measured illite "crystallinity" (*IC*) within the study region. Also, it is in accordance with the gradient established for the metamorphic subfacies notably from the extreme western Tassili n'Ajjer and emphasizes that illite crystallinity depends mainly on temperature. Using the model of Barker and Pawlewicz (1986), which has gained general acceptance for interpreting thermal histories of areas characterized by complex geological histories, the measured reflectance values which range between 1.09% and 1.84% VR_{eqv} correspond to a paleotemperature range of ~165–232 °C. These paleotemperatures estimates increased steadily westwards across the Tassili n'Ajjer, i.e., with a median of 171 °C, 172 °C, and 217 °C to the IMH, TAJ, and TAG sections, respectively (Table 3).

Source rock analyses of the Oued Imihrou Formation samples also demonstrated correlation with the previous thermal maturity evolution, such as the Production Index $[S_1/(S_1+ S_2)]$ with values > 0.1 (0.10–0.64, median = 0.34, n = 11) indicating an oil window. Also, the S_2 peak is the second peak in programmed pyrolysis that represents the hydrocarbon generative potential of the sample and this peak is used to

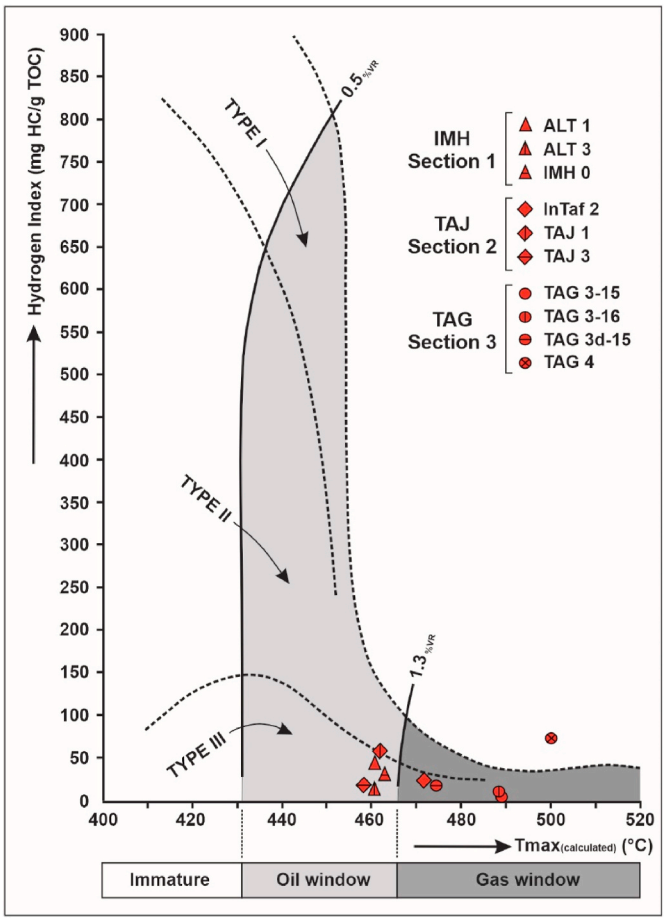

Fig. 8. Interpretation of kerogen types and maturity of the Oued Imihrou Formation black shales samples using the cross-plot of hydrogen index (HI) versus $T_{max(calculated)}$ temperature. The thermal maturity pathways, of all the analyzed samples, are plotted in the Type III kerogen region. TAG samples from the westernmost part of the Tassili n'Ajjer plateau have attained the gas window (Data in Table 3). Genetic paths for individual kerogen types after Espitalié (1986).

determine the $T_{max(Rock\text{-}Eval)}$ (°C) and thermal maturity of the rock (Espitalié et al., 1985; Espitalié, 1986; Peters and Cassa, 1994). Jarvie et al. (2001) and Laughrey (2014) derived almost the same conversion formula [%VR= (0.0180 * T_{max}) − 7.16] for the Barnett and Woodford shales, which has been used extensively for shale samples containing low-sulfur kerogen Type II and III, to determine the VR or $T_{max(calculated)}$ (°C) temperature. This relationship produces similar results to ours, except for a few samples (InTaf-2, TAJ-1, TAG-3d-15, and TAG-4). As a result of this, thermal maturity that is based on $T_{max(calculated)}$ ranges from the late oil window (≥460 °C) to early lower wet gas condensate (<475 °C). The highest values (474–500 °C), suggestive of the gas window, dry gas (methane) zones of hydrocarbon generation, and destruction, were found in the western sector of the study area (TAG section 3). The samples at this location also delivered good richness in organic matter and the residual TOC values vary from 0.48 to 2.09 wt% (median = 1.48, n = 4), cf. Table 3. Besides, these same shales northwards in the BGI basins have much higher TOC, i.e., an average of about 10 wt% with maximum values as high as 25 wt% (Lüning et al., 2000).

4.4. Illite K−Ar geochronology

Careful mineralogical analysis using the K−Ar age dating technique is of particular interest because it provides timing of diagenetic events even in complex geological settings (Clauer and Chaudhuri, 1995; Pevear, 1999; Uysal et al., 2001, 2004, 2006; Zwingmann et al., 1998, 2011). However, interpreting K–Ar analyses in terms of radiometric age requires some precautions as outlined by the review of Hamilton (2003) and Meunier et al. (2004).

The four ages from the Oued Imihrou Formation, (the eastern- and western-Tassili n'Ajjer plateau), were measured by the conventional K−Ar method on sub-fractions (<0.2 and < 0.1 μm); results are presented in Table 4. Lower K concentration in the four size fractions (median = 0.94%, n = 4) is caused probably by contamination with other mineral phases, such as quartz and kaolinite identified in the XRD analysis. All the determined ages seem to be significantly younger than the stratigraphic age of the host sediments (Early Silurian), with a large time span of about 155 Ma from Carboniferous to Lower Jurassic. With K−Ar ages younger than the stratigraphic age of their host rocks, the four dated sub-fractions cannot, of course, be of a strict detrital origin.

From the western Tassili, three ages are represented: 335.5 ± 8.0 Ma for the TAJ-0 sample and 238.3 ± 11.4 Ma for the TAG-3b-15 sample and an intermediate age 179.2 ± 4.3 Ma for the TAJ-4 sample. In addition, one age, from the eastern Tassili, yielded 204.1 ± 6.2 Ma for the ALT-1g sample. Therefore, at least two authigenic clay (illite) generations occurred in the separated size fractions, and both are logically expected to date older and younger diagenetic episodes. Interestingly, no major K−Ar ages have been detected after 179 Ma, which suggests that no further significant illite generations occurred after the Early Jurassic.

5. Discussion

5.1. Diagenetic- and thermal maturity-evolution in the Silurian formations

Most, if not all, of the identified illite minerals from Early Silurian Oued Imihrou black shales and the overlying Mid–Silurian sandstone levels of the Atafaïtafa Formation appear to be of authigenic, rather than, detrital origin. The presence of illite in all samples of the Silurian formations raises two questions: 1 – How are such illite particles formed? 2 – Under what conditions do these populations occur?

Illite is classically shown to occur systematically in all argillaceous series from a smectitic precursor via intermediate mixed-layer illite-smectite (I/S) through continuous reactions (Hower et al., 1976; Varajao and Meunier, 1995; Lanson et al., 1998; Meunier and Velde, 2004; Clauer and Liewig, 2013). In this study, the absence of expandable smectite layers and I/S with mostly *Ir* = 1 point to a final stage of the smectite-to-illite conversion, i.e., illitization processes, and hence *in situ* growing of illite flakes (Fig. 5A). This reaction mechanism involving illite formation from smectite by solid state transformation in diagenetic shales is characteristic of many deeply-buried sedimentary sequences at depths greater than 3–4 km (e.g. Eslinger and Pevear, 1988; Inoue et al., 1992; Velde and Vasseur, 1992; Eberl, 1993; Lanson et al., 1998, 2002; Merriman and Peacor, 1999; Meunier and Velde, 2004; Meunier, 2005). In contrast, the second population of pure illite (Fig. 5F), the overgrowth on the basal surfaces of detrital muscovite is of a different origin and did not form by burial diagenesis of smectite but was precipitated directly from hydrothermal fluids and illite dissolution-recrystallization at higher temperatures near or above 200 °C in conditions of anchizone (Laverret, 2002; Uysal et al., 2004; Zwingmann et al., 2010). This is consistent with the higher *IC* values ~0.53 Δ°2*θ*, and with a few samples (TAG: 2–16, 2c, 3a, 3d-15) already on the low anchizone boundary conditions (Table 1), as well as the higher graptolite reflectances VR_{eqv} 1.37–1.84% (Table 2), over the inherited N–S lineaments and mega-shear zones which were found to affect the westernmost part of the Tassili n'Ajjer plateau (Fig. 1B).

Besides the formation of the above-mentioned illites, the abundance of authigenic vermiform kaolinite would not persist under such high orogenic thermal conditions. Indeed, several studies have suggested that kaolinite precipitation is promoted at shallow-burial depth, while a

diagenetic kaolinite-to-dickite conversion is through the late diagenetic stage and incipient metamorphism (Beaufort et al., 1998; Cassagnabère et al., 1999; Lanson et al., 2002). Therefore, as non-morphology evolution from booklet to blocky was not observed, the preferred formation mechanism of 'late' stacked kaolinite is by direct precipitation or feldspar dissolution, which had to occur necessarily from meteoric-water flushing after the Hercynian orogeny and following the Cenozoic uplift of the Hoggar Massif. Moreover, these acidic meteoric waters, which are commonly diluted, oxidizing and saturated with CO_2, would have removed any unstable detrital minerals by several dissolutions, and hence explain the observed oversized pores within the Atafaïtafa Formation sandstones.

Throughout the three studied outcrop sections, both the thermal maturity determinations and graptolite reflectance data were accurately acquired on the graptolitic Early Silurian Oued Imihrou black shales in order to extract quantitative information on the degree of organic maturation, as well as the prevailing conditions (i.e. paleotemperatures) during the diagenetic illite precipitation and/or transformation. The study revealed that the good richness in organic matter and residual TOC content close to 2.5 wt% of predominantly kerogen Type II but behave like Type III is located in the west of the Tassili n'Ajjer plateau (Fig. 8). Indeed, as pointed out by Morga (2020) that elsewhere, the kerogen type of the graptolite periderm is frequently detected as transitive – II/III, although typical marine kerogen is of Type II, and Type III (represented by vitrinite) represents a terrestrial origin.

The thermal maturity of the graptolitic Early Silurian shales from the IMH, TAJ and TAG sections, i.e., VR_{eqv} values of 1.13–1.16, 1.09–1.34 and 1.37–1.84%, coincides broadly with the zones of oil and wet-gas with condensate formation, respectively. According to Barker and Pawlewicz (1986), such reflectance values indicate median paleotemperatures of ca. 152, 145 and 187 °C, respectively (Table 3). At least a 3-km- thick stratigraphic overburden, now almost completely eroded after the Hercynian- and Alpine-orogeny, was probably responsible for producing temperatures in the range of 140–160 °C with a 'normal' paleo-geothermal gradient of around 25–35 °C km^{-1} within the Algerian Sahara (cf. Makhous and Galushkin, 2003; Zieliński, 2012). Further to the westernmost part of the Tassili n'Ajjer, which is mainly affected by inherited transtensional Pan-African N–S f of some hundreds of kilometers long, higher maturities ($T_{max(calculated)}$ = 474–500 °C, gas maturity window) and maximum paleotemperatures in excess of 200 °C are recorded. Simultaneously, and as discussed above, the occurrence of 2*M* authigenic illite from TAJ and TAG could be explained by the evolution of illite to muscovite of Hunziker et al. (1986) and the 1*M*–2M_1 polytypic conversion of Frey (1987), Yang and Hesse (1991).

In summary, we demonstrated that the apparent discrepancy between the degree of thermal transformation of the sedimentary organic matter and the *in situ* neocrystallization of illites were genetically controlled by burial diagenesis and the highlighted lateral paleothermal gradient towards the West (Table 3). The repeatedly reactivated N–S lineaments and mega-shear zones in the Hoggar Massif, during the Phanerozoic orogeneses and rifting phases, constituted migration pathways for hydrothermal potassium-rich fluids, and in turn, induced thermal anomaly or brief 'heat spike' conjointly with diagenetic precipitation of illite crystals and organic maturation. In this respect, Takherist and Lesquer (1989), Yahi et al. (2001), later Makhous and Galushkin (2003) also highlighted very high heat-flow values (90–130 mW m^{-2}) compared to the world average (64 mW m^{-2}), notably along the Amguid-El Biod-Messaoud axis and the BGI sedimentary basins depocentres 'palaeo-kitchens'. These authors concluded that the elevated heat-flow within these areas may have played a crucial role in the thermal maturity of the Early Silurian black shales, with a hydrocarbon generation that began in the Early Carboniferous (Visean), persisted throughout the Triassic–Early Cretaceous, and the Late Cretaceous (Senonian). Hydrocarbon generation and migration in association with hydrothermal processes is well documented (Simoneit, 1992, 2020). There is a major difference in the effect on organic maturation between hydrothermal processes at high heating rates, and those obtained in step-wise, subsiding basins with sediment burial over prolonged geological times. Pulsed hydrocarbon generation occurs in sedimentary systems being affected by hydrothermal events, as opposed to an oil window of a sedimentary package in prolonged burial-related geological systems (Simoneit, 1992, 2020). Hydrothermal processes have been shown to be highly efficient in organic matter alteration or maturation, and hydrothermal petroleum formation should be considered in exploration for energy resources (Didyk and Simoneit, 1989; Simoneit et al., 2000).

5.2. *K–Ar timing and genesis of the illitic clays*

The first preliminary K–Ar results (Table 4), on at least two generations of authigenic micrometric illite-type crystals, document periods of fluid flow and, therefore, reconstruct for the first time the timing of the repeatedly intraplate fault reactivations within the Tassili n'Ajjer plateau at the northern Hoggar Shield (Fig. 1B).

K–Ar geochronology of illitic clay minerals from the Tassili indicates that the illite genesis was multi-phased with crystallization episodes at 335 ± 8 Ma (~ Middle Mississippian 'Visean'), 238 ± 11 Ma (Mid–Upper Triassic) and 204 ± 6 to 179 ± 4 Ma (Upper Triassic to Lower Jurassic).

The older illite of 335 ± 8 Ma is consistent with the timing of the early Hercynian tectono-thermal activity in the region, accompanied probably by the first hydrocarbon generation from the basal Silurian black 'hot' shales prior to the uplift, as identified in the BGI basins by early work of Tissot et al. (1973) and later on by Takherist et al. (1995); Makhous and Galushkin (2003). Clauer et al. (2019) also demonstrated that the Hercynian event, which is often of a hyper-volcanic type, started around 340 ± 10 Ma through the Hassi-Messaoud field in Algeria.

The intermediate age of illite crystallization at 238 ± 11 Ma could be attributed to an episodic thermal event through the studied area and elsewhere in Algeria. Indeed, the extensional tectonics that occurred during the Triassic (Tethys) rifting was at the origin of numerous syn-depositional volcanics in southeastern Algeria "Algerian Triassic Basin" (Boudjema, 1987; Guiraud, 1998; Turner et al., 2001).

While around the Triassic–Jurassic transition, the younger illite crystallizations at 204 ± 6 and 179 ± 4 Ma constrains most probably the faulting and magmatism of the Liassic phase, following the development of the Central Atlantic Magmatic Province (CAMP). Logan and Duddy (1998) and Chabou et al. (2007) reported from the Azzel Matti Ridge, the Ahnet and Reggane basins some doleritic sills of up to 15–20 m in thickness, as well as layered plutons. Their $^{40}Ar/^{39}Ar$ plateau ages show the peak of magmatic activities or thermal anomalies 'heat spike' at 192.7 ± 3 Ma and 198.9 ± 1.8 Ma.

Interestingly, no major K–Ar ages have been detected after 179 Ma, which suggests that no further significant illite generations occurred after the Early Jurassic. According to Clauer et al. (2019), the younger ages of illite at about 170 ± 10 Ma can be considered to have recorded significant hydrocarbon invasion that, in turn, had to inhibit any subsequent illitization reactions.

6. Summary and conclusions

The Tassili n'Ajjer plateau is the southern margin of the Berkine – Ghadames and Illizi "BGI" basins, e.g., the largest hydrocarbon-producing province in Algeria. These Lower Paleozoic outcrops along the Tassili n'Ajjer area provide a critical insight into understanding the diagenesis- and thermal maturity-evolution of the Silurian unconventional hydrocarbon deposits. Thus, while using multiple techniques and independent approaches, such as X-ray diffraction, electron microscopy, organic petrography, programmed Rock-Eval pyrolysis, and illite K–Ar geochronology.

The identified clay minerals include kaolinite, mica-illite, and chlorite. All these appear to be completely authigenic rather than of detrital

origin. The important differences in mineralogy depend on the stratigraphical level, geographical location, and lithology.

The authigenic illites in the Silurian of the Tassili n'Ajjer plateau are of different origin and did not form solely by burial diagenesis of smectite alone but were formed during multiple episode of heating and diagenetic fluid flow processes in response to various tectonic events.

Illite crystallinity *IC* indicates that alteration occurred within the deep diagenetic to anchi-metamorphic zones. The westernmost part of the Tassili n'Ajjer succession yielded the lowest *IC* values, around or less than 0.53 $\Delta°2\theta$: indicating high-temperature conditions of advanced grade diagenesis during illite crystallizations, and few samples already attained the low anchizone boundary.

The measured graptolite reflectance (GR_{omax} 1.14–2.59%), and Rock-Eval measurements for the exposed Silurian succession are consistent with the calculated paleotemperature range, spanning from late oil window ($T_{max(calculated)} \geq 460$ °C) through the condensate and wet gas phase to the dry gas (methane) zones (~500 °C) of hydrocarbon generation and destruction. Indeed, the maximum reflectance and highest estimates of paleotemperature (VR_{eqv} value of 1.84% and T = 232 °C) are observed along the mega-shear zones in the westernmost part of the Tassili n'Ajjer plateau, and much higher are likely to occur in the subsurface, i.e., northwards in the BGI basins. These highest values reflect an elevated thermal maturity westwards, clearly induced by large-scale hydrothermal activity in the study area.

The combined use of inorganic and organic thermal indicators, i.e., authigenic clay minerals and graptolite particles, as well as illite K−Ar geochronology, successfully demonstrated at least two heating events and diagenetic fluid flow processes. It is obvious that these events and processes later influenced hydrocarbon maturation, migration and/or entrapment, notably along the same major Precambrian N–S lineaments and Hoggar Massif inherited mega-shear zones that were repeatedly reactivated throughout the Phanerozoic.

K–Ar dating revealed the oldest illite ages of about 335 ± 8 Ma that fits within the timing of the early Hercynian tectono-thermal activity in the region, probably accompanied by the first hydrocarbon generation (i.e. Carboniferous age 'Visean'). The youngest illite crystallizations at 238 ± 11 Ma (Mid–Upper Triassic) and 204 ± 6 to 179 ± 4 Ma (Triassic–Jurassic transition) can be related to extensive thermal anomaly 'heat spike', and additional hydrocarbon charge from the Silurian source rock, following the Tethys rifting and the later development of the Central Atlantic Magmatic Province "CAMP", respectively.

The results of this study are the first documentation of the reactivation of Pan-African fault systems in south-eastern Algeria based on geochronology and graptolite reflectance. These reactivations may represent significant transtensional tectonic events coupled with subsequent igneous activity both during the opening of the Tethys (Triassic) and the Central Atlantic (Jurassic) oceans. Finally, the highest possibility of finding more hydrocarbon accumulations in south-eastern Algeria is to focus exploration mostly along the western margin of the BGI basins, i.e., areas bordering major lineaments.

Credit author Statement

Dr. H. Djouder (drafting the article, substantial contribution to: conception, design, acquisition of data, analysis, interpretation of data, and revising the article for important intellectual content); Dr. I.T. Uysal (drafting the article, substantial contribution to: conception, design, analysis, interpretation of data, and revising the article for important intellectual content); Dr. A.C. Da Silva (substantial contribution to analysis and interpretation of data); Dr. J. Bourdet (substantial contribution to acquisition of data); Dr. A. Todd (substantial contribution to acquisition of data); Dr. E. Ramanaïdou (drafting the article); Dr. B. Lamouri (substantial contribution to acquisition of data); Dr. P. Crosdale (substantial contribution to: acquisition of data, analysis, interpretation of data, and revising the article for important intellectual content); Prof. F. Boulvain (drafting the article).

Declaration of competing interest

The authors declare that they have no known competing financial interests or personal relationships that could have appeared to influence the work reported in this paper.

Data availability

Data will be made available on request.

Acknowledgements

The authors acknowledge the OPNT - UNESCO Tassili National Park management for their collaboration, providing logistics and invaluable assistance during the multiple fieldwork campaigns. We also wish to thank the Algerian Ministry of Culture for permission to conduct research and collect samples. Inspiring discussions and suggestions offered by Prof. J. Środoń (Polish Academy of Sciences), Dr. P. Hackley (USGS), and many colleagues are greatly appreciated. This work was funded partially by the University of Liège - Belgium [ARD Grants, FE0057/2016] awarded to Dr. H. Djouder. Also, Dr. A.C. Da Silva is financially supported by the Belgian National Science Foundation project [FNRS-T.0051.19]. This manuscript is a contribution to the IGCP-652 ("Reading geologic time in Paleozoic sedimentary rocks"). The authors are particularly grateful to the four anonymous reviewers for their critical but constructive and valuable comments that significantly enhanced the quality and language of this manuscript. This work belongs to the "Natural gas resources of Africa and Middle East and adjacent regions" special issue organized by the MPG journal and edited by Dr. A. Radwan and Dr. D. Wood.

References

Abad, I., 2007. Physical Meaning and Applications of the Illite Kübler Index: Measuring Reaction Progress in Low-Grade Metamorphism. Seminarios de la Sociedad Española de Mineralogía, pp. 53–64.

Abdelsalam, M.G., Liégeois, J.P., Stern, R.J., 2002. The saharan metacraton. J. Afr. Earth Sci. 34, 119–136.

Árkai, P., 1991. Chlorite crystallinity: an empirical approach and correlation with illite crystallinity, coal rank and mineral facies as exemplified by Palaeozoic and Mesozoic rocks of northeast Hungary. J. Metamorph. Geol. 9, 723–734.

Bailey, S.W., 1984. Classification and structures of micas. In: Bailey, S.W. (Ed.), Micas. Reviews in Mineralogy and Geochemistry, Mineralogical Society of America, Washington, D.C, v. 13, pp. 1–12.

Barker, C.E., Pawlewicz, M.J., 1986. The correlation of vitrinite reflectance with maximum paleotemperature in humic organic matter. In: Buntebarth, G., Stegena, L. (Eds.), Paleogeothermics. Springer-Verlag, New York, pp. 79–93.

Beaufort, D., Cassagnabere, A., Petit, S., Lanson, B., Berger, G., Lacharpagne, J.C., Johansen, H., 1998. Kaolinite-to-dickite conversion series in sandstone reservoirs. Clay Miner. 33, 297–316.

Behar, F., Beaumont, V., Penteado, H.L., De, B., 2001. Rock-Eval 6 technology: performances and developments. Oil Gas Sci. Technol. 56, 111–134.

Bekkouche, D., 1992. Le silurien Supérieur-Dévonien Inférieur du Bassin de Ghadamès (Sahara Oriental Algérien). Lithostratigraphie, sédimentologie et diagenèse des réservoirs.. Université de Grenoble 1, France [Ph.D. thesis], p. 311.

Beuf, S., Biju-duval, B., De Charpal, O., Rognon, P., Gariel, O., Bennacef, A., 1971. Les grès du Paléozoïque Inférieur du Sahara. Sédimentologie et Discontinuités. Evolution Structurale d'un Craton. Publication Institut Français de Pétrole (IFP), p. 464. Editions Technip, 18.

Bonhomme, M.G., Thuizat, R., Pinault, Y., Clauer, N., Wendling, R., Winkler, R., 1975. Méthode de datation potassium-argon. Appareillage et technique. Notes Tech. Inst. Geol., Univ. Louis Pasteur, Strasbourg, p. 53.

Boote, D.R., Clark-Lowes, D.D., Traut, M.W., 1998. Paleozoic petroleum systems of North Africa. In: Macgregor, D.S., Moody, R.T.J., Clark-Lowes, D.D. (Eds.), Petroleum Geology of North Africa, v. 132. Geological Society, pp. 7–69. London, Special Publication.

Boudjema, A., 1987. Evolution Structurale du Bassin Pétrolier "Triasique" du Sahara Nord Occidental (Algérie). Université Pierre et Marie Curie-Paris, France [Ph.D. thesis].

Brindley, G.W., Brown, G., 1980. Crystal Structures of Clay Minerals and Their X-Ray Identification. Mineral Soc, London, p. 495.

Carr, I.D., 2002. Second-order sequence stratigraphy of the palaeozoic of North Africa. J. Petrol. Geol. 25, 259–280.

Cassagnabère, A., Iden, I.K., Johansen, H., Lacharpagne, J.C., Beaufort, D., 1999. Kaolinite and dickite in froy and rind sandstone hydrocarbon reservoirs (brent

formation from norwegian continental shelf). In: 11th Intern Clay Conf Proc., Ottawa, pp. 97–102.
Chabou, M.C., Sebaï, A., Féraud, G., Bertrand, H., 2007. 40Ar/39Ar dating of the central atlantic magmatic province (CAMP) in southwestern Algeria. Compt. Rendus Geosci. 339, 970–978.
Clauer, N., Chaudhuri, S., 1995. Clays in the Crustal Environment: Isotope Dating and Tracing. Springer, Berlin, p. 359.
Clauer, N., Liewig, N., 2013. Episodic and simultaneous illitization in oil-bearing Brent Group and Fulmar Formation sandstones from the northern and southern North Sea based on illite K-Ar dating. AAPG (Am. Assoc. Pet. Geol.) Bull. 97, 2149–2171.
Clauer, N., Zwingmann, H., Todd, A., Aubert, A., 2019. Potassium-argon timing of episodic mica and illite crystallization in highly indurated Hassi Messaoud (Algeria) hydrocarbon-bearing sandstones. AAPG (Am. Assoc. Pet. Geol.) Bull. 103, 215–240.
Craig, J., Rizzi, C., Said, F., Thusu, B., Lüning, S., Asbali, A.I., Keely, M.L., Bell, J.F., Durham, M.J., Eales, M.H., Beswetherick, S., Hamblett, C., 2008. Structural styles and prospectivity in the precambrian and palaeozoic hydrocarbon systems of North Africa. In: Salem, M.J., Oun, K.M., Essed, A.S. (Eds.), The Geology of East Libya, vol. 4. Gutenberg Press, Malta, pp. 51–122.
Dalrymple, G.B., Lanphere, M.A., 1969. Potassium-Argon Dating. W. H. Freeman, San Francisco, p. 258.
Derder, M.E.M., Maouche, S., Liégeois, J.P., Henry, B., Amenna, M., Ouabadi, A., Bellon, H., Bruguier, O., Bayou, B., Bestandji, R., Nouar, O., Bouabdallah, H., Ayache, M., Beddiaf, M., 2016. Discovery of a Devonian mafic magmatism on the western border of the Murzuq basin (Saharan metacraton): paleomagnetic dating and geodynamical implications. J. Afr. Earth Sci. 115, 159–176.
Djouder, H., Murat, B., Musial, G., Lüning, S., Boulvain, F., 2015. Silurian-devonian black shales in the oriental Algerian Sahara: implication of new field data from the Tassili n'Ajjer outcrops and berkine basin (SE, Algeria). Oral session. In: Petroleum Source Rocks" specialized meeting by the French Geological Society (SGF) and TOTAL, Paris, France 2015. http://hdl.handle.net/2268/188644.
Djouder, H., Lüning, S., Da Silva, A.-C., Abdallah, H., Boulvain, F., 2018. Silurian deltaic progradation, Tassili n'Ajjer plateau, south-eastern Algeria: sedimentology, ichnology and sequence stratigraphy. J. Afr. Earth Sci. 142, 170–192.
Djouder, H., 2019. Silurian succession from North Africa: sedimentology, ichnology and thermal history for a new Era of hydrocarbon exploration. University of Liège, Belgium [Ph.D. thesis], p. 320. https://hdl.handle.net/2268/240479.
Didyk, B.M., Simoneit, B.R.T., 1989. Hydrothermal oil of Guaymas Basin and implications for petroleum formation mechanisms. Nature 342, 65–69.
Dong, H., Peacor, D.R., Freed, R.L., 1997. Phase relations among smectite, R1 illite-smectite, and illite. Am. Mineral. 82, 379–391.
Eberl, D.D., Velde, B., 1989. Beyond the Kübler index. Clay Miner. 24, 571–577.
Eberl, D.D., 1993. Three zones for illite formation during burial diagenesis and metamorphism. Clay Clay Miner. 41, 26–37.
English, K.L., Redfern, J., Bertotti, G., English, J.M., Yahia Cherif, R., 2016. Intraplate uplift: new constraints on the Hoggar dome from the Illizi basin (Algeria). Basin Res. 29, 1–17.
Eschard, R., Abdallah, H., Braik, F., Desaubliaux, G., 2005. The Lower Paleozoic succession in the Tassili outcrops, Algeria: sedimentology and sequence stratigraphy. First Break 23, 27–38.
Eschard, R., Braik, F., Bekkouche, D., Ben Rahuma, M., Desaubliaux, G., Deschamps, R., Proust, J.N., 2010. Palaeohighs: their influence on the North African Palaeozoic petroleum systems. In: Vining, B.A., Pickering, S.C. (Eds.), Petroleum Geology: from Mature Basins to New Frontiers – Proceedings of the 7th Petroleum Geology Conference. Geological Society, London, pp. 707–724.
Eslinger, E., Pevear, D., 1988. Clay Minerals for Petroleum Geologists and Engineers. SEPM Short Course Notes, vol. 22. Society of Economic Paleontologists and Mineralogists, Tulsa ix + p. 405.
Espitalié, J., Deroo, G., Marquis, F., 1985. La pyrolyse Rock-Eval et ses applications (deuxième partie). Revue Institut Français du Pétrole 40, 755–784.
Espitalié, J., 1986. Use of Tmax as a maturity index for different types of organic matter: comparison with reflectance. In: Bums, J. (Ed.), Thermal Modelling in Sedimentary Basins. Technip, Pans, pp. 475–496.
Fabre, J., 2005. Géologie du Sahara Occidental et Central. Tervuren Afr. Geosci. Collect. Mus. R. de l'Afr. Cent., Tervuren, Belgium 108, 572.
Fekirine, B., Abdallah, H., 1998. Palaeozoic lithofacies correlatives and sequence stratigraphy of the Saharan Platform, Algeria. In: MacGregor, D.S., Moody, R.T.J., Clark-Lowes, D.D. (Eds.), Petroleum Geology of North Africa, vol. 132. Geological Society, London, Special Publications, pp. 265–281.
Ferreiro Mählmann, R., Frey, M., 2012. Standardisation, calibration and correlation of the Kübler-Index and the vitrinite/bituminite reflectance: an inter-laboratory and field related study. Swiss J. Geosci. 105, 153–170.
Ferreiro Mählmann, R., Bozkaya, Ö., Potel, S., Le Bayon, R., Šegvić, B., Nieto, F., 2012. The pioneer work of Bernard Kübler and Martin Frey in very low-grade metamorphic terranes: paleo-geothermal potential of variation in Kübler-Index/organic matter reflectance correlations. A review. Swiss J. Geosci. 105, 121–152.
Franks, S.G., Zwingmann, H., 2010. Origin and timing of late diagenetic illite in the Permian-Carboniferous Unayzah sandstone reservoirs of Saudi Arabia. AAPG (Am. Assoc. Pet. Geol.) Bull. 94, 1133–1159.
Frey, M., 1987. Very low-grade metamorphism of clastic sedimentary rocks. In: Frey, M. (Ed.), Low Temperature Metamorphism. Blackie & Sons, Glasgow, pp. 9–58.
Galeazzi, S., Point, O., Haddadi, N., Mather, J., Druesne, D., 2010. Regional geology and petroleum systems of the Illizi–Berkine area of the Algerian Saharan Platform: an overview. Mar. Petrol. Geol. 27, 143–178.
Galushkin, Y.I., Makhous, M., 2006. Contribution of erosion and intrusive-hydrothermal activity to the depth profile of organic matter maturation in sedimentary basins. Geochem. Int. 44, 1225–1236.
Goodarzi, F., 1984. Organic petrography of graptolite fragments from Turkey. Mar. Petrol. Geol. 1, 202–210.
Goodarzi, F., Norford, B.S., 1987. Optical properties of graptolite epiderm – a review. Bull. Geol. Soc. Den. 35, 141–147.
Goodarzi, F., Norford, B.S., 1989. Variation of graptolite reflectance with depth of burial. Int. J. Coal Geol. 11, 127–141.
Goodarzi, F., Fowler, M.G., Bustin, M., McKirdy, D.M., 1992. Thermal maturity of Early Palaeozoic sediments as determined by the optical properties of marine-derived organic matter – a review. In: Schilowski, M., Golubic, S., Kimberley, M.M., McKirdy, D.M., Trudinger, P.A. (Eds.), Early Organic Evolution: Implications for Mineral and Energy Resources. Springer Verlag, pp. 279–295 (IGCP volume).
Guggenheim, S., Bain, D.C., Bergaya, F., Brigatti, M.F., Drits, A., Eberl, D.D., Formoso, M. L.L., Galán, E., Merriman, R.J., Peacor, D.R., Stanjek, H., Watanabe, T., 2002. Report of the Association Internationale pour l'Etude des Argiles (AIPEA) Nomenclature Committee for 2001: order, disorder and crystallinity in phyllosilicates and the use of the "Crystallinity Index". Clay Miner. 37, 389–393.
Guiraud, R., 1998. Mesozoic rifting and basin inversion along the northern African Tethyan margin: an overview. In: MacGregor, D.S., Moody, R.T.J., Clark-Lowes, D.D. (Eds.), Petroleum Geology of North Africa, vol. 132. Geological Society, London, Special Publications, pp. 217–229.
Guiraud, R., Doumnang Mbaigane, J.-C., Carretier, S., Dominguez, S., 2000. Evidence for a 6000 km length NW-SE striking lineament in northern Africa: the Tibesti lineament. J. Geol. Soc. 157, 897–900. London.
Guiraud, R., Bosworth, W., Thierry, J., Delplanque, A., 2005. Phanerozoic geological evolution of northern and central Africa: an overview. J. Afr. Earth Sci. 43, 83–143.
Hackley, P.C., Araujo, C.V., Borrego, A.G., Bouzinos, A., Cardott, B.J., Cook, A.C., Eble, C., Flores, D., Gentzis, T., Gonçalves, P.A., Mendonça Filho, J.G., Hámor-Vidó, M., Jelonek, I., Kommeren, K., Knowles, W., Kus, J., Mastalerz, M., Menezes, T. R., Newman, J., Oikonomopoulos, I.K., Pawlewicz, M., Pickel, W., Potter, J., Ranasinghe, P., Read, H., Reyes, J., De La Rosa Rodriguez, G., Alves Fernandes de Souza, I.V., Suárez-Ruiz, I., Sýkorová, I., Valentine, B.J., 2015. Standardization of reflectance measurements in dispersed organic matter: results of an exercise to improve interlaboratory agreement. Mar. Petrol. Geol. 59, 22–34.
Haddoum, H., Guiraud, R., Moussine-Pouchkine, A., 2001. Hercynian compressional deformations of the ahnet-mouydir basin, Algerian saharan platform: far-field stress effects of the late palaezoic orogeny. Terra. Nova 13, 220–226.
Hamilton, P.J., 2003. A review of radiometric dating techniques for clay mineral cements in sandstones. In: Worden, R., Morad, S. (Eds.), Clay Mineral Cements in Sandstones. Special Publication Number 34 of the International Association of Sedimentologists. Blackwell, Oxford, pp. 253–287.
Hartkopf-Fröder, C., Königshof, P., Littke, R., Schwarzbauer, J., 2015. Optical thermal maturity parameters and organic geochemical alteration at low grade diagenesis to anchimetamorphism: a review. Int. J. Coal Geol. 150–151, 74–119.
Hess, J.C., Lippolt, H.J., 1994. Compilation of K-Ar measurements on HD-B1 standard biotite. In: Odin, G.S. (Ed.), Phanerozoic Time Scale, Bull. Liaison Inf., vol. 12. IUGS Subcomm. Geochronology, pp. 19–23.
Hoffkecht, A., 1991. Mikropetrographische, Organisch-geochemische, Mikrothermometrische und Mineralogische Untersuchungen zur Bestimmung der Organische Reife von Graptholithen Periderm. Gottinger Arb. Geol. Palaontol. 48, 1–98.
Hoffman, J., Hower, J., 1979. Clay mineral assemblages as low grade metamorphic geothermometers: application to the thrust faulted disturbed belt of Montana. In: Scholle, P.A., Schluger, P.S. (Eds.), Aspects of Diagenesis, vol. 26. Special Publications, Society of Economic Paleontologists and Mineralogists, Tulsa, Oklahoma, USA, pp. 55–79.
Hower, J., Eslinger, E.V., Hower, M.E., Perry, E.A., 1976. Mechanism of burial metamorphism of argillaceous sediment: 1. Mineralogical and chemical evidence. Geol. Soc. Am. Bull. 87, 725–737.
Hunziker, J.C., Frey, M., Clauer, N., Dallmeyer, R.D., Friedrichsen, H., Flehmig, W., Hochstrasser, K., Roggwiler, P., Schwander, H., 1986. The evolution of illite to muscovite: mineralogical and isotopic data from the Glarus Alps. Switzerland. Contr. Min. Pet 92, 157–180.
İnan, S., Goodarzi, F., Schmidt-Mumm, A., Arouri, K., Qathami, S., Ardakani, O.H., İnan, T., Tuwailib, A.A., 2016. The silurian qusaiba hot shales of Saudi arabia: an integrated assessment of thermal maturity. Int. J. Coal Geol. 159, 107–119.
Inoue, A., Utada, M., Wakita, K., 1992. Smectite-to-illite conversion in natural hydrothermal systems. Appl. Clay Sci. 7, 131–145.
ISO 7404-3, 2009. Methods for the Petrographic Analysis of Coals–Part 3: Methods of Determining Maceral Group Composition. International Organization for Standardization, Geneva, Switzerland.
ISO 7404-5, 2009. Methods for the Petrographic Analysis of Coals–Part 5: Methods of Determining Microscopically the Reflectance of Vitrinite. International Organization for Standardization, Geneva, Switzerland, p. 14.
Jarvie, D., Claxton, B., Henk, F., Breyer, J., 2001. Oil and Shale Gas from the Barnett Shale, Fort Worth Basin, Texas, vol. 10. AAPG Ann. Meet. Progr, p. A100.
Kisch, H.J., 1987. Correlation between indicators of very low grade metamorphism. In: Frey, M. (Ed.), Low Temperature Metamorphism. Blackie & Sons, Glasgow, pp. 227–300.
Kisch, H.J., Árkai, P., Brime, C., 2004. On the calibration of the illite Kübler-Index (illite "crystallinity"). In: Schweizerische Mineralalogische und Petrographische Mitteilungen, v. 84, pp. 323–331.
Klemme, H.D., Ulmishek, G.F., 1991. Effective petroleum source rocks of the world: stratigraphic distribution and controlling depositional factors. Bull. Am. Assoc. Petrol. Geol. 75, 1809–1851.

Kübler, B., 1967. La cristallinité de l'illite et les zones tout à fait supérieures du métamorphisme. In: Étages tectoniques, Colloque de Neuchâtel, 18-21 avril 1966. A la Baconnière, Neuchâtel, Suisse, pp. 105–121.
Kübler, B., 1968. Evaluation quantitative du métamorphisme par la cristallinité de l'illite. Bull. Centre Recherche Pau, S.N.P.A. 2, 385–397.
Kübler, B., Jaboyedoff, M., 2000. Illite cristallinity. In: Comptes rendus de l'Académie des Sciences Paris Série II, v. 331, pp. 75–89.
Kuuskraa, V., Stevens, S., Van Leeuwen, T., Moodhe, K., 2011. World Shale Gas Resources: an Initial Assessment of 14 Regions outside the United States. Advanced Resources International for US Department of Energy, p. 365.
Lafargue, E., Marquis, F., Pillot, D., 1998. Rock-Eval 6 applications in hydrocarbon exploration, production, and soil contamination studies. Oil Gas Sci. Technol. 53, 421–437.
Lanson, B., Velde, B., Meunier, A., 1998. Late-stage diagenesis of illitic clay minerals as seen by decomposition of X-ray diffraction patterns: contrasted behaviors of sedimentary basins with different burial histories. Clay Clay Miner. 46, 69–78.
Lanson, B., Beaufort, D., Berger, G., Bauer, A., Cassagnabere, A., Meunier, A., 2002. Authigenic kaolin and illitic minerals during burial diagenesis of sandstones: a review. Clay Miner. 37, 1–22.
Laughrey, C.D., 2014. Introductory geochemistry for shale gas, condensate-rich shales and tight oil reservoirs. In: URTeC Annual Meeting Short Course. Colorado Convention Center, Denver, Colorado, p. 325.
Laverret, E., 2002. Evolutions temporelles et spatiales des alterations argileuses des gisements d'uranium sous discordance, secteur de Shea Creek (Bassin de l'Athabasca, Canada). Université de Poitiers, France [Ph.D. thesis], p. 192.
Lee, J.Y., Marti, K., Severinghaus, J.P., Kawamura, K., Yoo, H.S., Lee, J.B., Kim, J.S., 2006. A redetermination of the isotopic abundances of atmospheric Ar. Geochem. Cosmochim. Acta 70, 4507–4512.
Liégeois, J.P., Benhallou, A., Azzouni-Sekkal, A., Yahiaoui, R., Bonin, B., 2005. The hoggar swell and volcanism: reactivation of the precambrian Tuareg shield during alpine convergence and west African cenozoic volcanism. In: Foulger, G.R., Natland, J.H., Presnall, D.C., Anderson, D.L. (Eds.), Plates, Plumes and Paradigms, vol. 388. Geological Society of America Special Paper, pp. 379–400.
Liégeois, J.P., Abdelsalam, M.G., Ennih, N., Ouabadi, A., 2013. Metacraton: nature, genesis and behavior. Gondwana Res. 23, 220–237.
Link, C.M., Bustin, R.M., Goodarzi, F., 1990. Petrology of graptolites and their utility as indices of thermal maturity in lower Paleozoic strata in northern Yukon, Canada. Int. J. Coal Geol. 15, 113–135.
Logan, P., Duddy, I., 1998. An investigation of the thermal history of the Ahnet and Reggane basins, central Algeria, and the consequences for hydrocarbon generation and accumulation. In: MacGregor, D.S., Moody, R.T.J., Clark-Lowes, D.D. (Eds.), Petroleum Geology of North Africa, vol. 132. Geological Society, London, Special Publications, pp. 131–155.
Luo, Q., Zhong, N.N., Zhang, Y., Dai, Na, Zhang, W., 2016. Graptolite-derived organic matter in the Wufeng-Longmaxi formations (Upper Ordovician-Lower Silurian) of southeastern Chongqing, China: implications for gas shale evaluation. Int. J. Coal Geol. 153, 87–98.
Luo, Q., Goodarzi, F., Zhong, N., Wang, Y., Qiu, N., Skovsted, C.B., Suchý, V., Schovsbo, N.H., Morga, R., Xu, Y., Hao, J., Liu, A., Wu, J., Cao, W., Min, X., Wu, J., 2020. Graptolites as fossil geo-thermometers and source material of hydrocarbons: an overview of four decades of progress. Earth Sci. Rev. 200, 103000.
Lüning, S., Craig, J., Loydell, D.K., Storch, P., Fitches, W.R., 2000. Lowermost Silurian 'hot shales' in North Africa and Arabia: regional distribution and depositional model. Earth Sci. Rev. 49, 121–200.
MacGregor, D.S., 1998. Giant fields, petroleum systems and exploration maturity of Algeria. In: MacGregor, D.S., Moody, R.T.J., Clark-Lowes, D.D. (Eds.), Petroleum Geology of North Africa, vol. 132. Geological Society, London, Special Publications, pp. 79–96.
Makhous, M., Galushkin, YuI., 2003. Burial history and thermal evolution of the southern and western Saharan basins: synthesis and comparison with the eastern and northern Saharan basins. Am. Assoc. Petrol. Geol. Bull. 87, 1799–1822.
Merriman, R., Frey, M., 1999. Patterns of very low-grade metamorphism in metapelitic rocks. In: Frey, M., Robinson, D. (Eds.), Low Grade Metamorphism. Blackwell Science, Cambridge, pp. 61–107.
Merriman, R.J., Peacor, D.R., 1999. Very low-grade metapelites: mineralogy, microfabrics and measuring reaction progress. In: Frey, M., Robinson, D. (Eds.), Low-Grade Metamorphism. Blackwell Science, Oxford, pp. 10–60.
Meunier, A., Velde, B., 2004. Illite: Origins, Evolution and Metamorphism. Springer, Berlin, p. 286.
Meunier, A., Velde, B., Zalba, P., 2004. Illite K-Ar dating and crystal growth processes in diagenetic environments: a critical review. Terra. Nova 16, 296–304.
Meunier, A., 2005. Clays. Springer-Verlag, Berlin Heidelberg, p. 457.
Moore, D.M., Reynolds Jr., R.C., 1997. X-Ray Diffraction and the Identification and Analysis of Clay Minerals, second ed. Oxford University Press, p. 378.
Morga, R., 2020. Chemical properties of the graptolite periderm from the holy cross mountains (Central Poland). Bull. Geosci. 95, 205–213.
Mukhopadhyay, P.K., 1994. Organic Petrography and Kinetics of Limestone and Shale Source Rocks in Wells Adjacent to Sable Island, Nova Scotia and the Interpretation on Oil-Oil or Oil-Source Rock Correlation and Basin Modeling. Geological Survey of Canada, Open File Report, n° 3167.
Mullis, J., Stern, W.B., de Capitani, C., 1993. Correlation of fluid inclusion temperatures with illite, smectite and chlorite "crystallinity" data and smear slide chemistry in sedimentary rocks from the external parts of the Central Alps (Switzerland). In: IGCP Project 294, Very Low-Grade Metamorphism Symposium (Santiago de Chile).
Odin, G.S., 35 collaborators, 1982. Interlaboratory standards for dating purposes. In: Odin, G.S. (Ed.), Numerical Dating in Stratigraphy. Part 1. John Wiley and Sons, Chichester, pp. 123–148.
Perron, P., 2019. Architecture and tectonic of Paleozoic intracratonic Basins: impact on the sedimentary record and associated geometries. Example of peri-Hoggar Basins (North Gondwana marge). Université de Bourgogne Franche-Comté, France [Ph.D. thesis], p. 396.
Peters, K.E., Cassa, M.R., 1994. Applied source rock geochemistry. In: Magoon, L.B., Dow, W.G. (Eds.), The Petroleum System from Source to Trap, vol. 60. Amer. Assoc. Petrol. Geol. Mem, pp. 93–120.
Petersen, H.I., Schovsbo, N.H., Nielsen, A.T., 2013. Reflectance measurements of zooclasts and solid bitumen in Lower Paleozoic shales, southern Scandinavia: correlation to vitrinite reflectance. Int. J. Coal Geol. 114, 1–18.
Pevear, D.R., 1999. Illite and hydrocarbon exploration. Proc. Nat. Acad. Sci. U. S. A. 96, 3440–3446.
Rougier, S., Missenard, Y., Gautheron, C., Barbarand, J., Zeyen, H., Pinna, R., Liégeois, J. P., Bonin, B., Ouabadi, A., Derder, M.E.M., Frizon De Lamotte, D., 2013. Eocene exhumation of the Tuareg shield (Sahara desert, Africa). Geology 41, 615–618.
Simoneit, B.R.T., 1992. Organic matter alteration and fluid migration in hydrothermal systems. In: Parnell, J. (Ed.), Geofluids: Origin, Migration and Evolution of Fluids in Sedimentary Basins, vol. 78. Geological Society Special Publication, pp. 261–274.
Simoneit, B.R.T., Aboul-Kassim, T.A., Tiercelin, J.J., 2000. Hydrothermal petroleum from lacustrine sedimentary organic matter in the East African Rift. Appl. Geochem. 15, 355–368.
Simoneit, B.R.T., 2020. Hydrothermal petroleum. In: Wilkes, H. (Ed.), Hydrocarbons, Oils and Lipids: Diversity, Origin, Chemistry and Fate, Handbook of Hydrocarbon and Lipid Microbiology. Springer Nature Switzerland, pp. 557–592.
Środoń, J., 1984. X-ray powder diffraction identification of illitic materials. Clay Clay Miner. 32, 337–349.
Środoń, J., Clauer, N., Eberl, D.D., 2002. Interpretation of K–Ar dates of illitic clays from sedimentary rocks aided by modeling. Am. Mineral. 87, 1528–1535.
Środoń, J., 2013. Identification and quantitative analysis of clay minerals. In: Bergaya, F., Theng, B.K.G., Lagaly, G. (Eds.), Handbook of Clay Science, Developments in Clay Science, v. 5, pp. 25–49.
Steiger, R.H., Jäger, E., 1977. Subcommission on Geochronology: convention on the use of decay constants in geo-and cosmochronology. Earth Planet Sci. Lett. 36, 359–362.
Suchý, V., Sandler, A., Slobodník, M., Sýkorová, I., Filip, J., Melka, K., Zeman, A., 2015. Diagenesis to very low-grade metamorphism in lower Palaeozoic sediments: a case study from deep borehole Tobolka 1, the Barrandian Basin, Czech Republic. Int. J. Coal Geol. 140, 41–62.
Takherist, D., Lesquer, A., 1989. Mise en évidence d'importantes variations régionales du flux de chaleur en Algérie. Can. J. Earth Sci. 26, 615–626.
Takherist, D., 1990. Structure crustale, subsidence mésozoïque et flux de chaleur dans les bassins nord-sahariens (Algérie): apport de la gravimétrie et des données de puits. Université des Sciences et Techniques du Languedoc, Montpellier, France [Ph.D. thesis], p. 239.
Takherist, D., Arezki, A., Mouaici, R., 1995. Characterization and evolution of Paleozoic rock organic matter in Algerian Central Sahara. Am. Assoc. Petrol. Geol. Bull. 79, 1251 (abstract).
Taylor, G.H., Teichmüller, M., Davies, A., Diessel, C.F.K., Littke, R., Robert, P., 1998. Organic Petrology. Gebrüder Borntraeger, Berlin, p. 704.
Teichmüller, M., 1958. Métamorphisme du charbon et prospection du pétrole. Revue de l'Industrie Minérale, Special Publication, pp. 99–113.
Teichmüller, M., 1986. Organic petrology of source rocks, history and state of the art. Org. Geochem. 10, 581–599.
Teichmüller, M., 1987. Organic material and very low-grade metamorphism. In: Frey, M. (Ed.), Low Temperature Metamorphism. Blackie, Glasgow and London, pp. 114–161.
Tissot, B.P., Espitale, J., Deroo, G., Tempere, C., Jonathan, D., 1973. Origin and migration of hydrocarbons in the eastern Sahara (Algeria). In: Proceedings of the 6th International Meeting of Organic Geochemistry. Rueil-Malmaison, pp. 315–334.
Turner, P., Pilling, D., Walker, D., Exton, J., Binnie, J., Sabaou, N., 2001. Sequence stratigraphy and sedimentology of the late triassic TAG-I (blocks 401/402, berkine basin, Algeria). Mar. Petrol. Geol. 18, 959–981.
Uysal, I.T., Glikson, M., Golding, S.D., Audsley, F., 2000. The thermal history of the Bowen Basin, Queensland, Australia: vitrinite reflectance and clay mineralogy of Late Permian coal measures. Tectonophysics 323, 105–129.
Uysal, I.T., Golding, S.D., Thiede, D.S., 2001. K-Ar and Rb-Sr dating of authigenic illite-smectite in Late Permian coal measures, Queensland, Australia: implication for thermal history. Chem. Geol. 171, 195–211.
Uysal, I.T., Glikson, M., Golding, S.D., Southgate, P.N., 2004. Hydrothermal control on organic matter alteration and illite precipitation, Mt Isa Basin, Australia. Geofluids 4, 131–142.
Uysal, I.T., Mutlu, H., Altunel, E., Karabacak, V., Golding, S.D., 2006. Clay mineralogical and isotopic (K-Ar, δ18O, δD) constraints on the evolution of the north anatolian fault zone, Turkey. Earth Planet Sci. Lett. 243, 181–194.
Varajao, A., Meunier, A., 1995. Particle morphological evolution during the conversion of I/S to illite in lower Cretaceous shales from Sergipe-Alagoas basin, Brazil. Clay Clay Miner. 43, 35–59.
Velde, B., Vasseur, G., 1992. Estimation of the diagenetic smectite-to-illite transformation in time-temperature space. Am. Mineral. 77, 967–976.
Warr, L.N., Rice, A.H.N., 1994. Interlaboratory standardization and calibration of clay mineral crystallinity and crystallite size data. J. Metamorph. Geol. 12, 141–152.
Warr, L.N., Ferreiro Mählmann, R., 2015. Recommendations for kübler index standardization. Clay Miner. 50, 283–286.
Yahi, N., Schaefer, R.G., Littke, R., 2001. Petroleum generation and accumulation in the Berkine Basin, eastern Algeria. AAPG Bull. 85, 1439–1467.

Yang, C., Hesse, R., 1991. Clay minerals as indicators of diagenetic and anchimetamorphic grade in an overthrust belt, External Domain of southern Canadian Appalachians. Clay Miner. 26, 211–231.
Zieliński, M., 2012. Conodont thermal alteration patterns in Devonian and Carboniferous rocks of the Ahnet and Mouydir basins (southern Algeria). Mar. Petrol. Geol. 38, 166–176.
Zwingmann, H., Clauer, N., Gaupp, R., 1998. Timing of fluid flow in a sandstone reservoir of the north German Rotliegend (Permian) by K–Ar dating of related hydrothermal illite. In: Parnell, J. (Ed.), Dating and Duration of Fluid Flow and Fluid–Rock Interaction, vol. 144. Geological Society, Special Publication, London, pp. 91–106.
Zwingmann, H., Mancktelow, N., Antognini, M., Lucchini, R., 2010. Dating of shallow faults: new constraints from the AlpTransit tunnel site (Switzerland). Geology 38, 487–490.
Zwingmann, H., Han, R., Ree, J.-H., 2011. Cretaceous reactivation of the Deokpori Thrust, Taebaeksan Basin, South Korea, constrained by K-Ar dating of clayey fault gouge. Tectonics 30, 1–13.